Oligomer formation from the gas-phase reactions of Criegee intermediates with hydroperoxide esters: mechanism and kinetics

Long Chen,[1,2] Yu Huang,*[1,2] Yonggang Xue,[1,2] Zhihui Jia,[3] Wenliang Wang[4]

[1] *State Key Lab of Loess and Quaternary Geology (SKLLQG), Institute of Earth Environment, Chinese Academy of Sciences (CAS), Xi'an, 710061, China*

[2] *CAS Center for Excellence in Quaternary Science and Global Change, Xi'an, 710061, China*

[3] *School of Materials Science and Engineering, Shaanxi Normal University, Xi'an, Shaanxi, 710119, China*

[4] *School of Chemistry and Chemical Engineering, Key Laboratory for Macromolecular Science of Shaanxi Province, Shaanxi Normal University, Xi'an, Shaanxi, 710119, China*

Submitted to *Atmospheric Chemistry & Physics*

*Corresponding author:

Prof. Yu Huang, E-mail address: huangyu@ieecas.cn

Abstract

Hydroperoxide esters, formed in the reactions of carbonyl oxides (also called Criegee intermediates, CIs) with formic acid, play a crucial role in the formation of secondary organic aerosol (SOA) in the atmosphere. However, the transformation mechanism of hydroperoxide esters in the presence of stabilized Criegee intermediates (SCIs) is not well understood. Herein, the oligomerization reaction mechanisms and kinetics of distinct SCIs (CH_2OO, *syn*-CH_3CHOO, *anti*-CH_3CHOO and $(CH_3)_2COO$) reactions with their respective hydroperoxide esters as well as with hydroperoxymethyl formate (HPMF) are investigated in the gas phase using quantum chemical and kinetics modeling methods. The calculations show that the addition reactions of SCIs with hydroperoxide esters proceed through successive insertion of SCIs into hydroperoxide ester to form oligomers that involve SCIs as the repeated chain unit. The saturated vapour pressure and saturated concentration of the formed oligomers decrease monotonically as the number of SCIs is increased. The exothermicity of oligomerization reactions decreases significantly when the number of methyl substituents increases, and the exothermicity of *anti*-methyl substituted carbonyl oxides is obviously higher than that of *syn*-methyl substituted carbonyl oxides. The –OOH insertion reaction is energetically more feasible than the –CH insertion pathway in the SCIs oligomerization reactions, and the barrier heights increase with increasing the number of SCIs added to the oligomer except *syn*-CH_3CHOO. For the reactions of distinct SCIs with HPMF, the barrier of –OOH insertion pathway shows a dramatic decrease when a methyl substituent occurs at the *anti*-position, while it reveals a significant increase when a methyl group is introduced at the *syn*-position and dimethyl substituent. Compared with the rate coefficients of the CH_2OO + HPMF reaction, the rate coefficients increase by about one order of magnitude when a methyl substituent occurs at the *anti*-position, whereas the rate coefficients decrease by 1-2 orders of magnitude when a methyl group is introduced at the *syn*-position. These new findings advance our current understanding on the influence of Criegee-chemistry on the formation and growth processes as well as the

51   chemical compositions of SOA.

1. Introduction

Alkenes are an important class of volatile organic compounds (VOCs) that are emitted into the atmosphere from large quantities of biogenic and anthropogenic sources (Lester and Klippenstein, 2018). The reaction with ozone is one of the dominant degradation pathways for alkenes in the atmosphere (Johnson and Marston, 2008; Atkinson and Arey, 2003). Ozonolysis of alkene proceeds through the electrophilic 1,3-cycloaddition of ozone to C=C bond of alkenes to form a primary ozonides (POZ), and then it rapidly decomposes into a carbonyl compound and a carbonyl oxide (also called Criegee intermediates, CIs) (Criegee, 1975; Osborn and Taatjes, 2015; Giorio et al., 2017). A part of the initially energized CIs ($\sim$ 37-50%) may promptly dissociate to OH radicals, which are thought to be an important nonphotolytic source of OH radicals in the atmosphere (Novelli et al., 2014; Liu et al., 2014). The remaining CIs ($\sim$ 63-50%) are collisionally stabilized prior to the thermal unimolecular decay (Lester and Klippenstein, 2018; Novelli et al., 2014; Anglada and Solé, 2016). The stabilized Criegee intermediates (SCIs) can proceed bimolecular reactions with various trace species such as H_2O, NO_2, SO_2, and HCOOH to generate secondary organic aerosol (SOA), thus profoundly influencing air quality, global climate and human health (Osborn and Taatjes, 2015; Khan et al., 2018; Lin and Chao, 2017; Liu et al., 2019; Chhantyal-Pun et al., 2018; Gong and Chen, 2021; Taatjes, 2017).

Formic acid (HCOOH), one of the most abundant carboxylic acids, has a significant influence on rainwater acidity in remote areas, where pH reduces by 0.25-0.5 in the presence of HCOOH (Stavrakou et al., 2012; Wang et al., 2020; Chaliyakunnel et al., 2016). It also plays an important role in the formation of cloud condensation nuclei (CCN), indirectly influencing radiative forcing and climate change (Yu, 2000). The primary sources of HCOOH include biomass burning, human activities, tropical and boreal forests, as well as the secondary sources involve the photochemical oxidation of non-methane hydrocarbons, such as ketene-enols, vinyl

alcohol, isoprene, and terpenoids (Stavrakou et al., 2012; Wang et al., 2020; Chaliyakunnel et al., 2016; So et al., 2014; Paulot et al., 2011). According to satellite measurements, the production of HCOOH is up to 100-120 Tg yr^{-1}, and the value is expected to increase due to the acceleration of industrialization and urbanization (Stavrakou et al., 2012). Recent kinetics measurements have revealed that the reaction with HCOOH is a more important loss process for SCI than is presently assumed, especially in terrestrial equatorial areas and in high SCI concentration areas (Welz et al., 2014; Chung et al., 2019). The formed hydroperoxide esters have been identified as the low-volatility and high-oxygenated compounds, contributing to the formation and growth of SOA (Welz et al., 2014; Vansco et al., 2021; Sakamoto et al., 2017; Riva et al., 2017).

Welz et al. (2014) directly determined the rate coefficients for the reactions of CH_2OO and CH_3CHOO with formic and acetic acid by employing multiplexed photoionization mass spectrometry and cavity-enhanced broadband ultraviolet absorption spectroscopy. They found that the measured rate coefficients are in the excess of 1.0×10^{-10} cm^3 molecule^{-1} s^{-1}, which are several orders of magnitude greater than those derived from previous experimental studies (Johnson et al., 2001; Tobias and Ziemann, 2001). Sipilä et al. conducted a competitive reaction kinetics experiment to investigate the reactions of acetone oxide ((CH_3)$_2$OO) with SO_2, HCOOH and CH_3COOH, and they concluded that the rate coefficients of the (CH_3)$_2$OO + HCOOH/CH_3OOH reactions are faster than that of the (CH_3)$_2$OO + SO_2 system by about three times (Sipilä et al., 2014). These high rate coefficients could make the reaction with carboxylic acids a substantial dominant chemical sink for carbonyl oxides in the atmosphere (Welz et al., 2014; Taatjes et al., 2019; Chhantyal-Pun et al., 2017). Quantum chemical calculations show that the reaction of CH_2OO with HCOOH proceeds through a facile transfer of hydrogen atom from the acidic OH group to the terminal oxygen of CH_2OO to form hydroperoxymethyl formate (HPMF) (Long et al., 2009; Vereecken, 2017; Porterfield et al., 2019). Chen et al. (2018) concluded the same by investigating the reactions of various carbonyl oxides with HCOOH that the barrierless 1,4-insertion reaction is the most favorable

pathway, and the primary products are hydroperoxide esters. Caravan et al. (2020) employed high-level ab initio CCSD(T)-F12 methods to study the reaction of methyl vinyl ketone oxide (MVK-oxide) with HCOOH, and they found that the barrierless net insertion of MVK-oxide into HCOOH leading to the formation of a functionalized hydroperoxide is dominant over fragmentation to produce an alkoxy radical and OH radicals. Moreover, oligomerization reactions with hydroperoxides and peroxy radicals are identified as one of the dominant loss processes for carbonyl oxides under atmospheric conditions (Sakamoto et al., 2013; Sadezky et al., 2008; Zhao et al., 2015; Chen et al., 2017 and 2019). All the above milestone investigations provide important information for understanding the chemistry of Criegee intermediate in the presence of carboxylic acids. However, to the best of our knowledge, there are few studies on the oligomerization reactions of SCIs with hydroperoxide esters, which are important with regard to organic new particle and cloud condensation nuclei formations. Moreover, the relationship between the reactivity of SCIs and the nature of substituents remains uncertain in the SCIs oligomerization reactions.

In the present study, we mainly focus on the oligomerization reaction mechanisms and kinetics of four carbonyl oxides reactions with their respective hydroperoxide esters as well as with HPMF by employing quantum chemical calculations and kinetics modeling methods. For the initiation reactions of carbonyl oxides with formic acid, four kinds of pathways including 1,4 O-H insertion, 1,2 O-H insertion, C-H insertion, and C=O cycloaddition are considered. For the oligomerization reactions of the successive insertion of carbonyl oxides into hydroperoxide esters, two types of reactions involving –OOH and –CH insertions are taken into account. The selected carbonyl oxides, including CH_2OO, *syn-*, *anti-*CH_3CHOO and $(CH_3)_2CHOO$, are anticipated upon the ozonolysis of ethylene, propylene, and 2,3-dimethyl-2-butene, whereas the hydroperoxide esters are assumed to arise from the bimolecular reactions of carbonyl oxides with formic acid in the atmosphere.

2. Computational details

2.1 Electronic structure and energy calculations

The geometries of all stationary points, including reactants (R), intermediates (IM), transition states (TS), and products (P), are optimized at the M06-2X/6-311+G(2df,2p) level of theory, since the M06-2X functional has the reliable performance for predicting thermochemistry, kinetics and hydrogen bonding interactions (Zhao and Truhlar, 2008). Harmonic vibrational frequencies are performed at the same level to verify the nature of transition state (NIMAG = 1) and minimum (NIMAG = 0), and to provide zero-point vibrational energy (ZPVE) and Gibbs free energies corrections (G_{corr}), which are scaled by a factor of 0.98 (Alecu et al., 2010). Intrinsic reaction coordinate (IRC) calculations are carried out to verify that each transition state is connected to the desired reactant and product (Fukui, 1981). The single point energy (SPE) calculations are performed at the M06-2X/ma-TZVP level of theory based on the M06-2X/6-311+G(2df,2p) optimized geometries. Moreover, the basis set superposition error (BSSE) is performed by using the counterpoise method proposed by Boys and Bernardi (1970) to evaluate the stability of the pre-reactive complex (RC). Herein, the Gibbs free energy (G) is defined as the sum of SPE and Gibbs correction ($G = E + G_{corr}$). Electronic energy ($\Delta E^{\neq}$) and Gibbs free energy ($\Delta G^{\neq}$) barriers are defined as the difference in energy between a TS and a RC ($\Delta E^{\neq} = E_{TS} - E_{RC}$ and $\Delta G^{\neq} = G_{TS} - G_{RC}$). Reaction Gibbs free energy (ΔG) is defined as the difference in energy between a P and a R ($\Delta G = G_{P} - G_{R}$).

To further assess the reliability of the selected M06-2X/ma-TZVP method for SPE calculations, the single point energies of all stationary points involved in the initiation reactions of distinct SCIs with HCOOH are recalculated at the high-accuracy CCSD(T)/6-311+G(2df,2p) and QCISD(T)/6-311+G(2df,2p) levels of theory. The calculated results are summarized in Table S1. This table shows that the $\Delta E^{\neq}$ and $\Delta G^{\neq}$ obtained using the QCISD(T) method are in excellent agreement with those obtained using the CCSD(T) approach. It is therefore that the energies obtained using the CCSD(T) method are used as the benchmark for comparation. The mean

absolute deviations (MAD) of $\Delta E^{\neq}$ and $\Delta G^{\neq}$ between the CCSD(T) and M06-2X

methods are 0.43 and 0.41 kcal mol^{-1}, respectively; the largest deviations of $\Delta E^{\neq}$ and

$\Delta G^{\neq}$ are 1.0 and 1.1 kcal mol^{-1}, respectively. These results reveal that the energies

obtained using the M06-2X method are close to those obtained using the CCSD(T)

approach. Therefore, the M06-2X/ma-TZVP method is suitable to investigate the

SCIs oligomerization reactions. In the following discussion, the energies are applied

in terms of Gibbs free energy to describe the reaction mechanism unless otherwise

stated. All electronic structure calculations are carried out by using Gaussian 09

program (Frisch et al., 2009). The Multiwfn program and Visual molecular dynamics

(VMD) are utilized to analysis and visualize the molecular orbitals of the relevant

species (Lu and Chen, 2012; Humphrey et al., 1996).

2.2 Kinetics calculations

The rate coefficients for the barrierless 1,4 O-H insertion reactions are computed

by employing the variable-reaction-coordinate variational transition-state theory

(VRC-VTST) (Bao and Truhlar, 2017), in which the potential energies are calculated

by direct dynamics using the M06-2X/6-311+G(2df,2p) method. Rate coefficients for

the SCIs + HCOOH reactions are calculated using the E,J-resolved microcanonical

variational theory (E,J-μVT) using a single-faceted dividing surface. In the

VRC-VTST calculations, the reaction coordinate s is defined by pivot points, which

are used to orientate the reactants 1 and 2. s is defined as the minimal value of r_{ij},

where r_{ij} is the distance between pivot points i and j, i is a pivot point on reactant 1

and j is a pivot point on reactant 2. Two of the pivot points are located at a distance $\pm d$

from the center of mass (COM) of SCIs, and the other two pivot points are located at

a distance $\pm d$ from the COM of HCOOH with a fixed length of 0.05, 0.10, 0.15, 0.2

and 0.25 Å. Then, for a given choice of pivot points, the variationally lowest rate

coefficients are minimized with respect to s at each of the temperatures. We observed

that d=0.05 produces the best variation results and only its value is reported in the

present study.

The rate coefficients for the bimolecular reactions with the tight transition states

are calculated by using the canonical transition state theory (CTST) along with one-dimensional asymmetric Eckart tunneling correction (Truhlar et al., 1996; and Eckart, 1930). As shown in Fig. 1, the entrance pathway Entry2 of R_1R_2COO reaction with HCOOH consists of two steps: (i) an intermediate IMent2 is formed via a barrierless process; (ii) then, it rearranges to the product Pent2 through a tight transition state TSent2. The whole reaction process can be described as Eq. (1):

$$R_1R_2COO + HCOOH \underset{k_{-1}}{\overset{k_1}{\rightleftharpoons}} IMent2 \xrightarrow{k_2} Pent2 \qquad (1)$$

Assuming the rapid equilibrium is established between the IMent2 and reactants. According to the steady-state approximation (SSA), the total rate coefficient is approximately expressed as Eq. (2) (Zhang et al., 2012):

$$k_{tot} = \frac{k_1}{k_{-1} + k_2} k_2 \approx \frac{k_1}{k_{-1}} k_2 = K_{eq}k_2 \qquad (2)$$

The equilibrium constant K_{eq} is written as Eq. (3):

$$K_{eq} = \sigma \frac{Q_{IM}(T)}{Q_{R1}(T)Q_{R2}(T)} \exp\left(\frac{G_R - G_{IM}}{RT}\right) \qquad (3)$$

where σ refers to reaction symmetry number, $Q_{IM}(T)$, $Q_{R1}(T)$ and $Q_{R2}(T)$ denote the partition functions of intermediate, reactants R1 and R2, which are equal to the multiplication of translational, rotational, vibrational and electronic partition functions ($Q = Q_{rot}Q_{vib}Q_{trans}Q_{elec}$) (Mendes et al., 2014), T is the temperature in Kelvin, R is the ideal gas constant, G_R and G_{IM} are the total Gibbs free energies of reactant and intermediate, respectively. The rate coefficient calculations are performed with the Polyrate 2017-C and KiSThelP 2019 programs (Canneaux et al., 2013; Zheng et al., 2018).

3. Results and discussion

3.1 Initiation reactions of distinct SCIs with HCOOH

The reaction with HCOOH is one of the dominant loss processes for SCIs and is expected to trigger the formation of SOA in the atmosphere (Chhantyal-Pun et al., 2018; Cabezas and Endo, 2020; Zhao et al., 2018; Zhou et al., 2019). The potential

223   energy surface (PES) of distinct SCIs (CH_2OO, *syn*-, *anti*-CH_3CHOO and $(CH_3)_2COO$)

224   reactions with HCOOH is drawn in Fig. 1. The geometries of all stationary points are

225   displayed in Fig. S1. The relative free energy of each stationary point and free energy

226   barrier ($\Delta G^{\neq}$) of each elementary reaction are summarized in Table 1. As shown in Fig.

227   1, the bimolecular reaction of distinct SCIs with HCOOH proceeds via four possible

228   pathways, namely (1) 1,4 O-H insertion (Entry 1), (2) 1,2 O-H insertion (Entry 2), (3)

229   C-H insertion (Entry 3), and (4) C=O cycloaddition (Entry 4). For Entry 1, the

230   addition reaction of CH_2OO with HCOOH proceeds through the 1,4 O-H insertion of

231   CH_2OO into HCOOH to form a hydroperoxide ester $HC(O)O\text{-}CH_2OO\text{-}H$ with a

232   exoergicity of 37.6 $kcal \cdot mol^{-1}$. The formation of $HC(O)O\text{-}CH_2OO\text{-}H$ is obtained

233   through a concerted process of $O_2\text{-}H_2$ bond breaking in the HCOOH and $O_4\text{-}H_2$ and

234      $C_2\text{-}O_1$ bonds forming. Despite an attempt by various methods, the corresponding

235   transition state is still not located in the effort of optimization. To further validate the

236   barrierless process of 1,4 O-H insertion reaction, a relaxed scan over the O-H and C-O

237   bonds is performed at the M06-2X/6-311+G(2df,2p) level of theory. The scans start

238   from the optimized structure of the adduct products, and the O-H and C-O bond

239   lengths are then increased in steps of 0.10 Å, while other geometric parameters are

240   fully optimized. The zero of energy is set to be the energy of the adduct products. The

241   electronic potential energy profiles along the O-H and C-O dissociation coordinate are

242   presented in Fig. S2. As seen in Fig. S2a, the electronic potential energy of the

243   minimum potential-energy path (MEP) decreases monotonically when the bond

244   length of the O-H and C-O bonds decreases, suggesting that the 1,4 O-H insertion

245   reaction of CH_2OO with HCOOH is indeed barrierless. Similar conclusion is also

246   obtained from the electronic potential energy profiles for the *anti*-CH_3CHOO +

247   HCOOH, *syn*-CH_3CHOO + HCOOH and $(CH_3)_2COO$ + HCOOH (Fig. S2b-d)

248   reactions that 1,4 O-H insertion reactions are barrierless. This conclusion is further

249   supported by the analogous reaction systems that 1,4 O-H insertion reactions of

250   carbonyl oxides with carboxylic acids are a barrierless process including concerted

251   hydrogen atom transfer and new C-O bond formation (Chhantyal-Pun et al., 2017;

252   Long et al., 2009; Vereecken, 2017; Cabezas and Endo, 2019; Lin et al., 2019).

253   The exothermicities of 1,4 O-H insertion reactions of distinct SCIs with HCOOH

254   are assessed by the reaction enthalpies ($\Delta_r H^{\circ}_{298}$), which are defined as the difference

255   between the enthalpies of formation ($\Delta_f H^{\circ}_{298}$) of the products and reactants

256   ($\Delta_r H^{\circ}_{298} = \sum_{products} \Delta_f H^{\circ}_{298} - \sum_{reactants} \Delta_f H^{\circ}_{298}$). To the best of our knowledge, there are no literature

257   values available on the enthalpies of formation of carbonyl oxides and hydroperoxide

258   esters except the simplest carbonyl oxide CH_2OO. Therefore, the isodesmic reaction

259   method is adopted to obtain the enthalpies of formation, and the results are listed in

260   Table S2. An isodesmic reaction is a hypothetical reaction, in which the type of

261   chemical bonds in the reactants is the similar as that of chemical bonds in the products.

262   The following isodesmic reaction is constructed because the experimental values of

263   H_2, CH_4 and H_2O are available ($\Delta_f H^{\circ}_{298}(H_2) = 0.00$ kcal·mol^{-1}; $\Delta_f H^{\circ}_{298}(CH_4) = -17.82$

264   kcal·mol^{-1}; $\Delta_f H^{\circ}_{298}(H_2O) = -57.79$ kcal·mol^{-1}).

265    $$SCIs + nH_2 \rightarrow CH_4 + mH_2O \qquad (4)$$
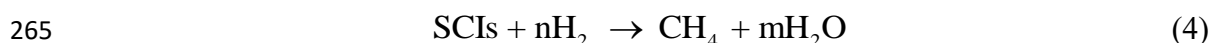
266   As seen in Table S2, the enthalpy of formation of CH_2OO is calculated to be

267   23.23 kcal·mol^{-1}, which is in good agreement with the available literature values

268   (Chen et al., 2016; Karton et al., 2013). This result implies that the theoretical method

269   employed herein is reasonable to predict the thermochemical parameters. The

270   enthalpies of formation of carbonyl oxides and hydroperoxide esters significantly

271   decrease with increasing the number of methyl groups. Notably, the decreased values

272   in the enthalpies of formation of carbonyl oxides are greater than those of

273   hydroperoxide esters under the condition of the same number of methyl groups. For

274   example, the enthalpy of formation of *anti*-CH_3CHOO decreases by 12.95 kcal·mol^{-1}

275   compared to the enthalpy of formation of CH_2OO (23.23 kcal·mol^{-1}), and the enthalpy

276   of formation of Pent1b decreases by 12.12 kcal·mol^{-1} compared to the enthalpy of

277   formation of Pent1a (-112.08 kcal·mol^{-1}). The reaction enthalpies of the reactions of

278   distinct SCIs with HCOOH decrease in the order of -44.69 (CH_2OO + HCOOH →

279   Pent1a) < -43.86 (*anti*-CH_3CHOO + HCOOH → Pent1b) < -38.13 (*syn*-CH_3CHOO +

280   HCOOH → Pent1c) < -37.12 kcal·mol^{-1} (($CH_3)_2COO$ + HCOOH → Pent1d),

indicating that the reaction enthalpies are highly dependent on the number and location of methyl groups. The trend in reaction enthalpies is consistent with the trend in the enthalpies of formation of carbonyl oxides.

For Entry 2, each addition reaction starts with the formation of a pre-reactive hydrogen bonded complex IMent2 in the entrance channel. Then it immediately converts into product Pent2 through the 1,2 O-H insertion transition state. The formation of Pent2 is obtained via a concerted process of O_2-H_2 bond rupture in the HCOOH and O_4-H_2 and C_2-O_2 bonds forming. The reaction barrier $\Delta G^{\neq}$ increases in the order of 10.0 (CH_2OO) < 13.0 (*anti*-CH_3CHOO) < 14.6 (*syn*-CH_3CHOO) $\approx$ 14.4 (($CH_3)_2COO$) kcal·mol^{-1}, suggesting that the parent CH_2OO + HCOOH reaction is favored kinetically. Compared with the barrier of the parent system, the barrier increases by 3.0 kcal·mol^{-1} when a methyl substitution occurs at the R_1 position, and the barrier increases by $\sim$ 5 kcal·mol^{-1} when a methyl group is introduced at the R_2 position and dimethyl substituent. The aforementioned result implies that the methyl-substituted CH_2OO hinders the 1,2 O-H insertion of carbonyl oxides into formic acid. Notably, the exothermicity decreases significantly as the number of methyl group is increased. The products Pent1 and Pent2 formed from Entry 1 and 2 are two conformations that differ in the orientation of the –C(O)H moiety over the –OOH group. The calculated result shows that Pent1 is more stable than Pent2 in energy due to the existence of intramolecular hydrogen bond between hydrogen atom of –OOH group and carbonyl oxygen atom.

For Entry 3, the addition reaction begins with the formation of a pre-reactive complex IMent3 in the entrance channel, and then it surmounts a barrier to reaction. However, the barriers of C-H insertion reactions are significantly high (21.8-27.6 kcal·mol^{-1}), such that they are of less importance in the atmosphere. The high reaction barriers might be attributed to the large bond dissociation energy (BDE) of C-H bond in the formic acid. For Entry 4, the addition reaction proceeds through a cyclization process of C_2-O_1 and O_4-C_1 bond forming to produce a five-membered ring compound Pent4. The barrier of C=O cycloaddition reaction in the CH_2OO + HCOOH reaction is 5.8 kcal·mol^{-1}, which is lower than that of the corresponding channels in Entry 2 and

Entry 3 by 4.2 and 16.0 kcal·mol^{-1}, respectively. The result reveals that the C=O cycloaddition reaction is feasible kinetically. A similar conclusion is also obtained from the reactions of HCOOH with syn-, $anti$-CH$_3$CHOO and (CH$_3$)$_2$COO that the C=O cycloaddition reactions are favored over 1,2 O-H and C-H insertion reactions.

The rate coefficients of each elementary pathway included in the initiation reactions of distinct SCIs with HCOOH are tabulated in Table S3-S6. The total rate coefficient is equal to the sum of the rate coefficient of each elementary pathway. As shown in Table S3, the total rate coefficients $k_{tot\text{-}CH2OO}$ of CH$_2$OO reaction with HCOOH are in excess of 1.0×10^{-10} cm^3 molecule^{-1} s^{-1}, and they exhibit a slightly negative temperature dependence in the temperature range of 273-400 K. At room temperature, $k_{tot\text{-}CH2OO}$ is estimated to be 1.29×10^{-10} cm^3 molecule^{-1} s^{-1}, which is in good agreement with the experimental values reported by Welz et al. (2014) ([1.1 ± 0.1] $\times 10^{-10}$), Chung et al. (2019) ([1.4 ± 0.3] $\times 10^{-10}$), and Peltola et al. (2020) ([1.0 ± 0.03] $\times 10^{-10}$). $k(TS_{ent1})$ is approximately equal to $k_{tot\text{-}CH2OO}$ in the whole temperature range, and it decreases in the range of 1.34×10^{-10} (273 K) to 1.05×10^{-10} (400 K) cm^3 molecule^{-1} s^{-1} with increasing temperature. $k(TS_{ent1})$ is several orders of magnitude greater than $k(TS_{ent2})$, $k(TS_{ent3})$ and $k(TS_{ent4})$ over the temperature range from 273 to 400 K. The result again shows that the barrierless 1,4 O-H insertion reaction is predominant. It should be noted that although the barrier of Entry 2 is 4.2 kcal·mol^{-1} higher than that of Entry 4, $k(TS_{ent2})$ is merely about 1-2 fold smaller than $k(TS_{ent4})$. The reason is ascribed to the fact that the C=O cycloaddition reaction is entropically unfavorable (Vereecken, 2017).

Equivalent to the case of the reaction of CH$_2$OO with HCOOH, the total rate coefficient $k_{tot\text{-}anti}$ of $anti$-CH$_3$CHOO reaction with HCOOH also decreases slightly with the temperature increasing (Table S4). This table shows that Entry 1 is kinetically favored over Entry 2, 3 and 4, and Entry 2 is competitive with Entry 4 in the temperature range of 273-400 K. Similar conclusion is also obtained from the results of the rate coefficients for the reactions of syn-CH$_3$CHOO and (CH$_3$)$_2$COO with HCOOH that Entry 1 is the dominant pathway (Table S5-S6). It deserves mentioning that the competition of Entry 2 is significantly greater than that of Entry 4

in the *syn*-CH_3CHOO + HCOOH and $(CH_3)_2COO$ + HCOOH systems. Based on the above discussions, it can be concluded that the relative importance of different pathways is highly dependent on the number and location of methyl substituents in the carbonyl oxides. Notably, the rate coefficient of each elementary pathway included in the *anti*-CH_3CHOO + HCOOH reaction is several orders of magnitude greater than that of the corresponding channel involved in the other SCIs + HCOOH systems. It is because that *anti*-CH_3CHOO is substantially more reactive toward HCOOH than other SCIs. Similar phenomenon has also observed from the reactivity of *anti*-CH_3CHOO toward water and SO_2 (Taatjes et al., 2013; Long et al., 2016; Huang et al., 2015; Cabezas and Endo, 2018). At ambient temperature, the total rate coefficients of HCOOH reactions with *anti*-CH_3CHOO, *syn*-CH_3CHOO and $(CH_3)_2COO$ are estimated to be 5.22, 2.18 and 3.97 $\times$ 10^{-10} cm^3 molecule^{-1} s^{-1}, respectively, which are consistent with the prior experimental measurements of 5 $\pm$ 3, 2.5 $\pm$ 0.3 and 4.5 $\pm$ 0.9 $\times$ 10^{-10} cm^3 molecule^{-1} s^{-1} (Welz et al., 2014; Sipilä et al., 2014).

In summary, the barrierless 1,4 O-H insertion reaction is the dominant pathway in the initiation reactions of distinct SCIs with HCOOH. This conclusion is consistent with the recent experimental results derived from the reactions of formic acid with methacrolein oxide (MACR-OO) and methyl vinyl ketone oxide (MVK-OO) that the 1,4-addition mechanism is energetically favorable (Vansco et al., 2021; Caravan et al., 2020). Therefore, in the present study, the adduct products Pent1 formed form the barrierless 1,4 O-H insertion of carbonyl oxides into HCOOH are selected as the model compounds to investigate the oligomerization reaction mechanisms of carbonyl oxides reactions with hydroperoxide esters.
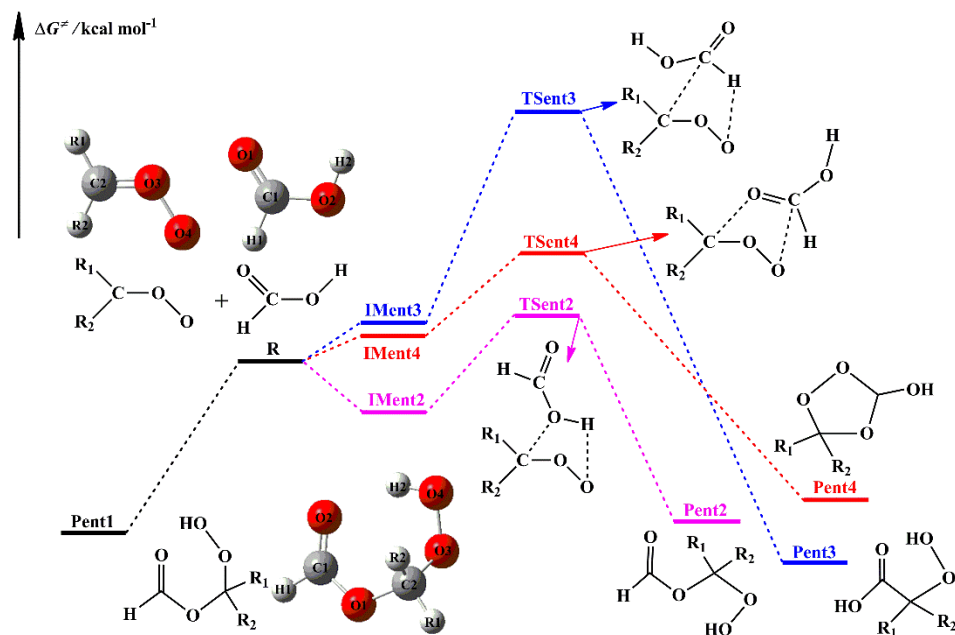
 Figure 1. Schematic PES for the possible entrance pathways of the initiation reactions of HCOOH
with various SCIs (black, pink, blue, and red lines represent 1,4 O-H insertion, 1,2 O-H insertion,
C-H insertion, and C=O cycloaddition reactions, respectively)

Table 1 Relative free energies of stationary points and free-energy barriers ($\Delta G^{\neq}$) at 298 K in kcal
mol^{-1} for the various SCIs (R_1R_2COO, R_1, R_2=H, CH$_3$) reactions with HCOOH calculated at the
M06-2X/ma-TZVP//M06-2X/6-311+G(2df,2p) level of theory

Entry	R1	R2	IMent	TSent	Pent	$\Delta G^{\neq}$
1	H	H	–	–	-37.6	–
	CH$_3$	H	–	–	-34.0	–
	H	CH$_3$	–	–	-29.8	–
	CH$_3$	CH$_3$	–	–	-25.6	–
2	H	H	-3.1	6.9	-37.3	10.0
	CH$_3$	H	-11.0	2.0	-33.7	13.0
	H	CH$_3$	-6.6	8.0	-29.1	14.6
	CH$_3$	CH$_3$	-8.8	5.6	-24.9	14.4
3	H	H	3.4	25.2	-46.9	21.8
	CH$_3$	H	1.8	24.0	-41.5	22.2
	H	CH$_3$	3.0	30.6	-37.6	27.6
	CH$_3$	CH$_3$	1.9	29.5	-33.0	27.6
4	H	H	3.4	9.2	-31.7	5.8
	CH$_3$	H	2.2	7.8	-29.4	5.6
	H	CH$_3$	3.5	14.6	-25.3	11.1
	CH$_3$	CH$_3$	3.0	13.2	-22.9	10.2

3.2. The reactions of distinct SCIs with their respective hydroperoxide esters

The formed hydroperoxide ester has two possible unimolecular decay pathways. The first is the direct O-O bond rupture resulting in the formation of oxylmethylformate and OH radicals (Vereecken, 2017). The second is the –OH fragment binding to adjacent hydrogen atom leading to the formation of anhydride and H_2O (Aplincourt and Ruiz-López, 2000; Neeb et al., 1998). However, the barriers of these two unimolecular reactions are extremely high, such that they are of less importance in the atmosphere. The formed hydroperoxide ester possess –OOH and –OC(O)H groups, both of them can serve as the reactive moieties to react with carbonyl oxides giving rise to the formation of oligomers. In the present study, we mainly consider two types of pathways: (a) –OOH insertion and (b) –CH insertion, while the C=O cycloaddition reaction is not taken into account because it is entropically unfavorable (Vereecken, et al., 2017; Lin et al., 2009). The aforementioned reactions are discussed in detail in the following subsections.

3.2.1 The reactions of 2CH$_2$OO with Pent1a

The simplest carbonyl oxide, CH_2OO, originates from the reaction of all terminal alkenes with ozone (ozonolysis) in the atmosphere (Lin and Chao, 2017). The reaction with HCOOH is expected to be one of the dominant loss processes for CH_2OO, and the main product is Pent1a (also called HPMF) (Welz et al., 2014; Cabezas and Endo, 2019). A schematic PES for the addition reaction $2CH_2OO$ + Pent1a is drawn in Fig. 2, and the optimized geometries of all stationary points are displayed in Fig. S3. As seen in Fig. 2, the successive insertion of CH_2OO into Pent1a eventually leads to the formation of oligomers P2a and P2b composed of CH_2OO as the repeat unit. These oligomerization reactions are strongly exothermic and spontaneous (> 83 kcal·mol^{-1}), implying that they are feasible thermodynamically.

The addition reaction $2CH_2OO$ + Pent1a initially proceeds through two possible pathways, namely (1) –OOH insertion reaction R1a, and (2) –CH insertion reaction R1b. For the –OOH insertion reaction R1a, the pre-reactive intermediate IM1a with a seven-membered ring structure is formed in the entrance channel, which is stabilized by the hydrogen bond interactions between the H_4 atom of Pent1a and the O_6 atom of

CH$_2$OO (D$_{(O6-H4)}$ = 1.706 Å), and between the H$_6$ atom of CH$_2$OO and the O$_3$ atom of Pent1a (D$_{(O3-H6)}$ = 2.115 Å). Then IM1a converts into P1a (C$_3$H$_6$O$_6$, HC(O)O–(CH$_2$OO)$_2$–H) via a concerted process of O$_4$-H$_4$ bond breaking in the Pent1a and O$_4$-C$_3$ and H$_4$-O$_6$ bonds forming with a barrier of 8.1 kcal·mol^{-1}. For the –CH insertion reaction R1b, the pre-reactive intermediate IM1b with a seven-membered ring structure is formed in the entrance channel, which is stabilized by the van der Waals (vdW) interactions between the O$_3$ atom of Pent1a and the C$_3$ atom of CH$_2$OO (D$_{(O3-C3)}$ = 2.602 Å), and between the O$_6$ atom of CH$_2$OO and the C$_1$ atom of Pent1a (D$_{(O6-C1)}$ = 2.608 Å). Due to the absence of hydrogen bond in IM1b, the energy of IM1b is lower than that of IM1a by 3.0 kcal·mol^{-1}. IM1b transforms into P1b (C$_3$H$_6$O$_6$, HO$_2$CH$_2$OC(O)CH$_2$OOH) via a concerted process of C$_1$-H$_1$ bond breaking in the Pent1a and C$_1$-C$_3$ and H$_1$-O$_6$ bonds forming with a barrier of 21.5 kcal·mol^{-1}. By comparing the barriers of R1a and R1b, it can be concluded that the –OOH insertion reaction is favored over the –CH insertion reaction. The high reaction barrier of R1b is attributed to the large bond dissociation energy (BDE) of C-H bond in the Pent1a. To further insight into the reaction mechanism of R1a, the natural bond orbital (NBO) analysis of the donor-acceptor orbitals involved in the TS1a is performed using the M06-2X wave function. The possible donor-acceptor interactions are estimated by using the second order perturbation theory. As illustrated in Fig. S4, the strong interactions are identified as the interaction of the lone pair orbital of O$_6$ atom and the antibonding orbital of O$_4$-H$_4$ bond, and the interaction of the lone pair orbital of O$_4$ atom and the antibonding orbital of C$_3$-O$_5$ bond.

Similarly, the addition reaction CH$_2$OO + P1a proceeds through the formation of the pre-reactive intermediates IM2a and IM2b in the entrance channel, which are stabilized by a hydrogen bond between the terminal oxygen atom of CH$_2$OO and the reacting hydrogen atom of P1a, and a van der Waals (vdW) interaction between the central carbon atom of CH$_2$OO and the carbonyl oxygen atom of P1a. The relative energies of IM2a and IM2b with respect to the separate reactants P1a and CH$_2$OO are -1.2 and 3.2 kcal·mol^{-1}, respectively, below the energies of the initial reactants 2CH$_2$OO and Pent1a are 41.6 and 37.2 kcal·mol^{-1}, respectively. Then they

433 immediately transform into the respective products P2a and P2b through the –OOH

434 and –CH insertion transition states TS2a and TS2b with the barriers of 10.1 and 21.6

435 kcal·mol^{-1}. This result again shows that the –OOH insertion reaction is favored

436 kinetically. It deserves mentioning that the barrier of –OOH insertion reaction

437 increases as the number of CH$_2$OO is increased. From the viewpoint of the

438 geometrical parameters of TS2a and TS2b, the breaking O-H and C-H bonds are

439 elongated by 14.8% and 20.6%, respectively, with respect to the equilibrium

440 structures of IM2a and IM2b, while the forming C-O and C-C bond length are 2.013

441 and 2.264 Å, respectively. The result reveals that TS2a and TS2b are structurally

442 reactant-like, which are consistent with the Hammond's hypothesis that the earlier

443 transition states are generally exothermic (Hammond, 1955).
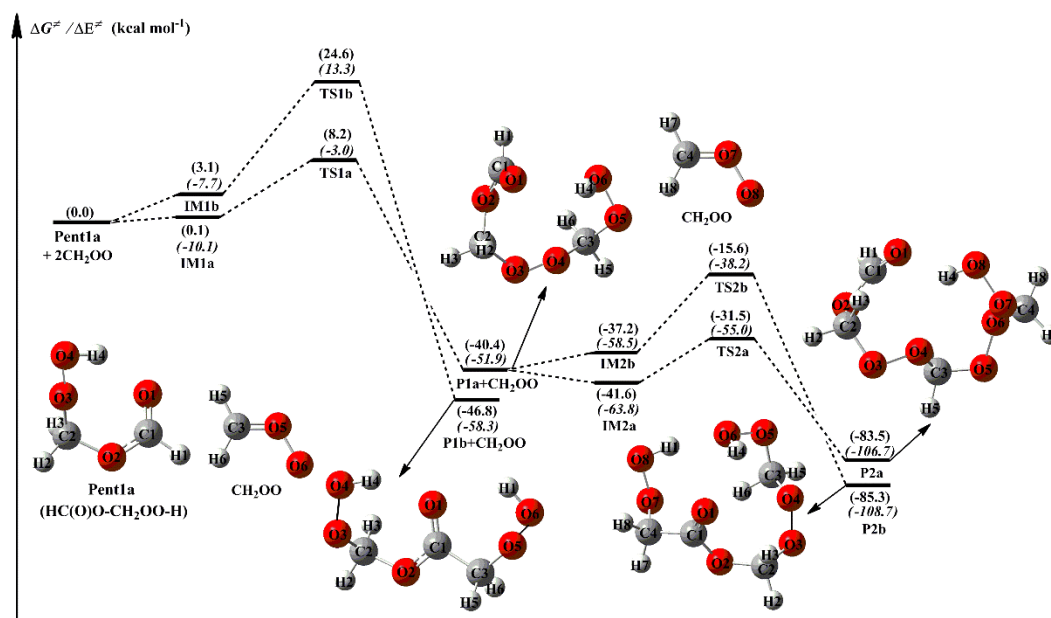
444
445 **Figure 2.** PES (ΔG and ΔE, in italics) for the 2CH$_2$OO + Pent1a reaction at the
446 M06-2X/ma-TZVP//M06-2X/6-311+G(2df,2p) level of theory

3.2.2 The reactions of *anti*-CH$_3$CHOO with Pent1b

448 The methyl-substituted CH$_2$OO has two conformers, *syn-* and *anti*-CH$_3$CHOO

449 that distinguish by the orientation of methyl group relative to the terminal oxygen

450 (Taatjes et al., 2013). *syn*-CH$_3$CHOO is more stable than *anti*-CH$_3$CHOO in energy

451 due to the existence of intramolecular hydrogen bond (Long et al., 2016). The

452 activation enthalpy of the interconversion between *syn*-CH$_3$CHOO and

453 *anti*-CH$_3$CHOO is up to 38.5 kcal·mol^{-1}, implying that they can treat as independent

454 species in the atmosphere (Long et al., 2016; Yin and Takahashi, 2017). A schematic

455 PES for the addition reaction 2*anti*-CH$_3$CHOO + Pent1b is presented in Fig. 3, and

456 the optimized geometries of all stationary points are shown in Fig. S5. As shown in

457 Fig. 3, the addition reaction 2*anti*-CH$_3$CHOO + Pent1b proceeds through successive

458 insertion of *anti*-CH$_3$CHOO into Pent1b leading to the formation of oligomers P4a

459 and P4b that contain *anti*-CH$_3$CHOO as chain unit. The first *anti*-CH$_3$CHOO addition

460 reaction begins with the formation of IM3a and IM3b in the entrance channel, which

461 lie -2.2 and 2.4 kcal·mol^{-1} respectively, with respect to the separate reactants. Then the

462 IM3a and IM3b transform into P3a and P3b via –OOH and –CH insertion transition

463 states TS3a and TS3b with the barriers of 5.6 and 20.3 kcal·mol^{-1}. This result shows

464 that the –OOH insertion reaction is more favorable than the –CH insertion pathway.

465 Compared with the barriers of R1a and R1b in the 2CH$_2$OO + Pent1a reaction, the

466 barriers of R3a and R3b decrease by 2.5 and 1.2 kcal·mol^{-1} when a methyl group is

467 introduced at the *anti*-position. The result reveals that the reactivity of

468 *anti*-CH$_3$CHOO is substantially higher than that of CH$_2$OO. This conclusion is further

469 supported by the findings of other studies, which have reported that *anti*-CH$_3$CHOO

470 is more reactive toward H$_2$O, SO$_2$, and H$_2$O$_2$ than CH$_2$OO (Chen et al., 2017; Taatjes

471 et al., 2013; Huang et al., 2015). Similarly, the secondary *anti*-CH$_3$CHOO addition

472 reaction starts with the formation of IM4a and IM4b in the entrance channel with the

473 0.1 and 3.7 kcal·mol^{-1} stability, followed by conversion to the final products P4a and

474 P4b through the –OOH and –CH insertion reactions R4a and R4b. The transition

475 states TS4a and TS4b lie 7.0 and 21.0 kcal·mol^{-1}, respectively, above the energies of

476 the respective intermediates IM4a and IM4b. This result again shows that the –OOH

477 insertion reaction is the most favorable channel, and the barrier increases as the

478 number of *anti*-CH$_3$CHOO is increased.

479
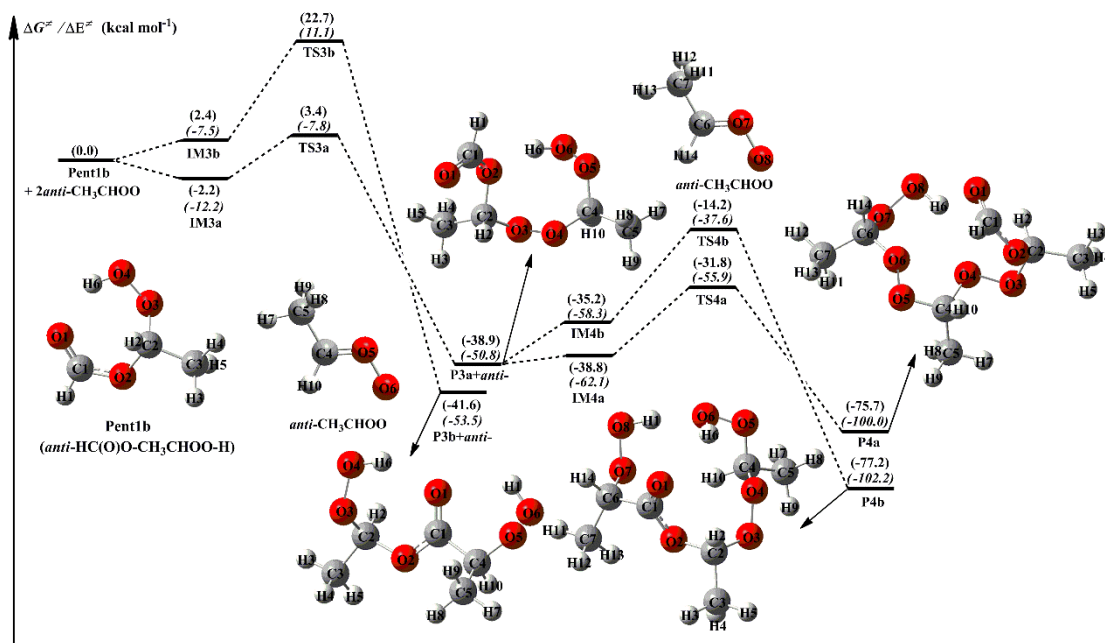
Figure 3. PES (ΔG and ΔE, in italics) for the 2*anti*-CH$_3$CHOO + Pent1b reaction at the M06-2X/ma-TZVP//M06-2X/6-311+G(2df,2p) level of theory

3.2.3 The reactions of *syn*-CH$_3$CHOO with Pent1c

Equivalent to the 2*anti*-CH$_3$CHOO + Pent1b reaction, the addition reaction 2*syn*-CH$_3$CHOO + Pent1c has similar transformation pathways, and is thus briefly discussed in the present study. From Fig. 4, it can be seen that the addition reaction 2*syn*-CH$_3$CHOO + Pent1c undergoes via successive insertion of *syn*-CH$_3$CHOO into Pent1c to form P6a and P6b that involve *syn*-CH$_3$CHOO as the repeating unit. The most favorable pathway is that the breakage of O$_4$-H$_6$ bond in the –OOH group of Pent1c occurs simultaneously with the insertion of first *syn*-CH$_3$CHOO into Pent1c to form P5a, followed by the insertion of secondary *syn*-CH$_3$CHOO into P5a to produce P6a. The barriers of these two –OOH insertion reactions R5a and R6a are 13.8 and 11.8 kcal·mol^{-1}, respectively, which are higher than those of R3a and R4a in the 2*anti*-CH$_3$CHOO + Pent1b system by 8.2 and 4.8 kcal·mol^{-1}, respectively. The result reveals that the reactivity of *syn*-CH$_3$CHOO is substantially lower than that of *anti*-CH$_3$CHOO. Notably, the barrier of the favorable –OOH insertion pathway decreases with increasing the number of *syn*-CH$_3$CHOO in the 2*syn*-CH$_3$CHOO + Pent1c reaction, which is contrary to the case of the 2CH$_2$OO + Pent1a and 2*anti*-CH$_3$CHOO + Pent1b reactions.
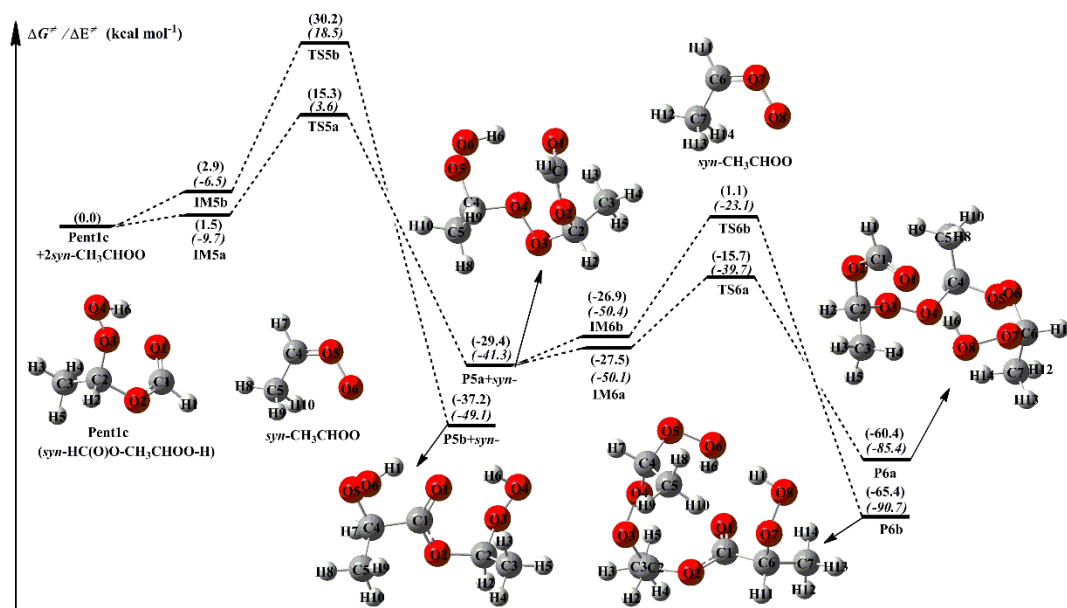
Figure 4. PES (ΔG and ΔE, in italics) for the $2syn$-CH$_3$CHOO + Pent1c reaction at the M06-2X/ma-TZVP//M06-2X/6-311+G(2df,2p) level of theory

3.2.4 The reactions of 2(CH$_3$)$_2$COO with Pent1d

The dimethyl-substituted Criegee intermediate, (CH$_3$)$_2$COO, is generated from the ozonolysis of 2,3-dimethyl-2-butene in the atmosphere (Lester and Klippenstein, 2018; Drozd et al., 2017; Long 2018). The bimolecular reaction of (CH$_3$)$_2$COO with water is not fast enough ($k < 1.5 \times 10^{-16}$ cm^3 molecule^{-1} s^{-1}), while the reaction of (CH$_3$)$_2$COO with HCOOH has a near gas kinetic limit rate ($k = 5.4 \times 10^{-10}$ cm^3 molecule^{-1} s^{-1}) (Huang et al., 2015). The result implies that a fraction of (CH$_3$)$_2$COO may survive under high humidity environments and react with HCOOH leading to the formation of hydroperoxide ester Pent1d. A schematic PES for the addition reaction 2(CH$_3$)$_2$COO + Pent1d is plotted in Fig. 5, and the optimized geometries of all stationary points are shown in Fig. S7.

As seen in Fig. 5, the addition reaction 2(CH$_3$)$_2$COO + Pent1d starts with the formation of complexes IM7a and IM7b, which lie 1.9 and 2.4 kcal·mol^{-1}, respectively, above the energies of the separate reactants. Then they subsequently transform into products P7a and P7b through the –OOH and –CH insertion transition states TS7a and TS7b with the barriers of 12.2 and 26.4 kcal·mol^{-1}. This result again shows that the –OOH insertion reaction is favored over the –CH insertion pathway. A similar conclusion is also obtained from the secondary (CH$_3$)$_2$COO addition reaction

520 that the –OOH insertion reaction is the dominant pathway. It is of interest to compare

521 the barriers of –OOH insertion reactions in the $(CH_3)_2COO$ + Pent1d system with

522 those of the analogous reactions in other SCIs + Pent1 reactions. It can be found that

523 the barriers decrease in the order of *syn*-CH_3CHOO > $(CH_3)_2COO$ > CH_2OO >

524 *anti*-CH_3CHOO in the first-step SCIs addition reaction, while they become

525 $(CH_3)_2COO$ > *syn*-CH_3CHOO > CH_2OO > *anti*-CH_3CHOO in the second-step SCI

526 addition pathway. The result shows that the reactivity of SCIs is significantly affected

527 by the number and location of methyl substituents. A similar conclusion is also

528 obtained from the thermodynamic parameters that the exothermicity of –OOH

529 insertion reactions significantly decreases with increasing the number of methyl

530 substituents, and the exothermicity of *anti*-methyl substituted carbonyl oxide is

531 obviously higher than that of *syn*-methyl substituted carbonyl oxide.
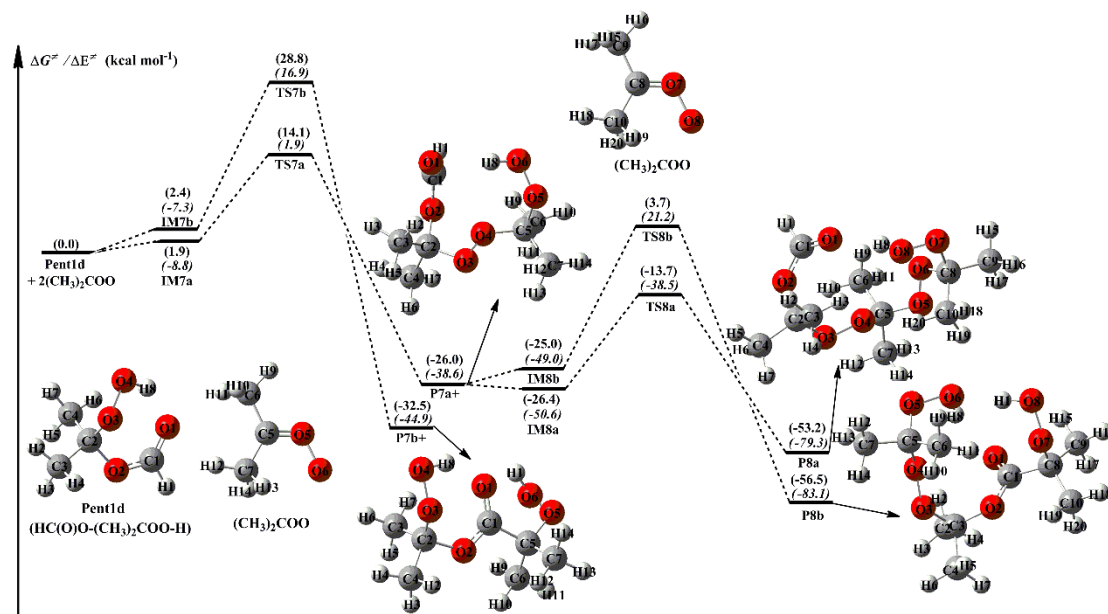
Figure 5. PES (ΔG and ΔE, in italics) for the $2(CH_3)_2COO$ + Pent1d reaction at the M06-2X/ma-TZVP//M06-2X/6-311+G(2df,2p) level of theory.

3.3 The reactions of distinct SCIs with Pent1a and implications in atmospheric chemistry

537 To further elucidate the effect of the number and location of methyl substituents

538 on the reactivity of carbonyl oxides toward hydroperoxide esters, Pent1a (also called

539 HPMF) is selected as the model compound since it is the simplest hydroperoxide ester

540 formed from the barrierless reaction of 1,4 O-H insertion of CH_2OO into HCOOH. As

mentioned above, –OOH insertion reaction in the oligomerization reactions is the most favorable pathway. Therefore, this type of reaction is merely considered in the reactions of distinct SCIs with Pent1a. The corresponding PES and the optimized geometries of all stationary points are displayed in Figs. 6 and S8, respectively. As seen in Fig. 6, each pathway starts with the formation of a pre-reactive intermediate, and then it overcomes a modest barrier to reaction. The barrier of the reaction of CH_2OO with Pent1a is calculated to be 8.1 kcal·mol^{-1}, which is higher than that of the *anti*-CH_3CHOO + Pent1a reaction by 2.5 kcal·mol^{-1}. The reason of low barrier can be explained by the NPA atomic charges, as presented in Fig. S9. As seen in Fig. S9, the charges of the central carbon atom C_1 and the terminal oxygen atom O_1 of CH_2OO are 0.186e and -0.459e, respectively, indicating that CH_2OO is indeed a zwitterion. The C_1 atom charge becomes more positive (0.393e), while the O_1 atom charge becomes more negative (-0.497e) when a methyl substituent occurs at the *anti*-position. This result suggests that the *anti*-methyl substituent enhances the characteristic of carbonyl oxides zwitterion and reduces the reaction barriers. Compared with the barrier of the CH_2OO + Pent1a reaction, the barriers increase by about 3.0 kcal·mol^{-1} when a methyl group is introduced at the *syn*-position and dimethyl substituent. Although *syn*-methyl and dimethyl substituent promote the raise of carbonyl oxides zwitterion, the steric hindrance effect and intramolecular hydrogen bond are obviously dominant for *syn*-CH_3CHOO and $(CH_3)_2COO$, that are not thus conducive to the nucleophilic attack of hydroperoxide esters. It is worth noting that the exothermicity of distinct SCIs reactions with Pent1a obviously decreases as the number of methyl group is increased, and the exothermicity of *anti*-methyl substituent is higher than that of *syn*-methyl substituent.

The rate coefficients of distinct SCIs reactions with Pent1a are calculated in the temperature range of 273-400 K as summarized in Table S7. This table shows that the rate coefficients k_{R1a} of the CH_2OO + Pent1a reaction (R1a) decrease in the range of 5.0×10^{-11} (273 K) to 5.0×10^{-12} cm^3 molecule^{-1} s^{-1} (400 K) with increasing temperature. A similar phenomenon is also observed from the rate coefficients of Pent1a reactions with *anti*-CH_3CHOO (R9), *syn*-CH_3CHOO (R10), and $(CH_3)_2COO$

571 (R11) that they exhibit a slightly negative temperature dependence. k_{R9} is several

572 orders of magnitude greater than k_{R1a}, k_{R10} and k_{R11} in the whole temperature range,

573 suggesting that the bimolecular reaction *anti*-CH$_3$CHOO + Pent1a (R9) is favored

574 kinetically. Compared with the rate coefficients of R1a, the rate coefficients increase

575 by about one order of magnitude when a methyl substituent occurs at the *anti*-position,

576 whereas the rate coefficients decrease by 1 to 2 orders of magnitude when a methyl

577 group is introduced at the *syn*-position. It should be noted that although the barrier of

578 R10 is nearly identical to that of R11, k_{R10} is 1 to 2 orders of magnitude lower than

579 k_{R11} in the entire temperature range. This is probably because the rate coefficients are

580 mediated by pre-reactive intermediates that IM11 is more stable than IM10 in energy.

581   It is of interest to assess whether the reactions of distinct SCIs with HPMF can

582 compete well with the losses to reactions with trace species (e.g., H$_2$O, HCOOH and

583 SO$_2$), because it is well known that the reactions with trace species are expected to be

584 the dominant chemical sinks for SCIs in the atmosphere (Taatjes et al., 2013; Long et

585 al., 2016). The reported concentrations of coreactant, the rate coefficients k, and the

586 effective pseudo-first-order rate constants ($k_{eff} = k$[coreactant]) for the reactions of

587 distinct SCIs with H$_2$O, HCOOH, SO$_2$, and HPMF are summarized in Table 2. As

588 seen in Table 2, the rate coefficient of a particular SCI reaction with trace species is

589 strongly dependent on its structure. The methyl group substitution may alter the rate

590 coefficient by several to tens of times. The atmospheric concentrations of H$_2$O,

591 HCOOH and SO$_2$ in the tropical forest environments are measured to be 3.9-6.1 $\times$

592 10^{17}, 5.0-10 $\times$ 10^{10}, and 1.7-9.0 $\times$ 10^{10} molecules cm^{-3}, respectively (Vereecken et al.,

593 2012). For the reactions of CH$_2$OO with H$_2$O, HCOOH, and SO$_2$, the experimental

594 rate coefficients are determined to be < 1.5 $\times$ 10^{-15}, [1.1 $\pm$ 0.1] $\times$ 10^{-10}, and [3.9 $\pm$ 0.7]

595 $\times$ 10^{-11} cm^3 molecule^{-1} s^{-1}, respectively (Welz et al., 2012 and 2014; Chao et al., 2015),

596 which translate into $k_{eff(CH2OO+H2O)}$, $k_{eff(CH2OO+HCOOH)}$ and $k_{eff(CH2OO+SO2)}$ of 5.9-9.2 $\times$

597 10^2, 5.5-11, and 0.7-3.5 s^{-1}, respectively. The result reveals that the reaction of

598 CH$_2$OO with H$_2$O is the most important bimolecular reaction. $k_{eff(CH2OO+HCOOH)}$ is

599 greater by a factor of 3-8 than $k_{eff(CH2OO+SO2)}$, indicating that CH$_2$OO reaction with

600 HCOOH is favored over reaction with SO$_2$. Similar conclusion is also obtained from

the results of k_{eff} for the reactions of *anti*-CH$_3$CHOO, *syn*-CH$_3$CHOO and (CH$_3$)$_2$COO with H$_2$O, HCOOH and SO$_2$ that SCIs reactions with H$_2$O are faster than with HCOOH, which, in turn, are faster than with SO$_2$.

According to the results shown in the Table 2, the room temperature rate coefficient for the reaction of CH$_2$OO with HPMF is calculated to be 2.7×10^{-11} cm^3 molecule^{-1} s^{-1}. However, to the best of our knowledge, the atmospheric concentration of HPMF has not been reported up to now. We assume that the concentration of HPMF is approximately equal to the atmospheric concentration of SCIs, since the SCIs is the deficient reactant in the bimolecular reaction of SCIs with HCOOH. Previous model-measurement studies have estimated the surface-level SCIs concentrations in the range of 1.0×10^4 to 1.0×10^5 molecules cm^{-3} (Khan et al., 2018; Novelli et al., 2017). $k_{eff(CH2OO+HPMF)}$ is calculated to be $2.7\text{-}27 \times 10^{-7}$ s^{-1}, which is several orders of magnitude lower than $k_{eff(CH2OO+H2O)}$, $k_{eff(CH2OO+HCOOH)}$ and $k_{eff(CH2OO+SO2)}$. Similar conclusion is also obtained from the reactions of *anti*-CH$_3$CHOO, *syn*-CH$_3$CHOO and (CH$_3$)$_2$COO with HPMF.

To further evaluate the relative importance of the complex SCIs reactions with coreactant, the bimolecular reactions of methyl vinyl ketone oxide (MVK-OO) with H$_2$O, HCOOH, SO$_2$, and HPMF are taken into account. MVK-OO, formed with 21 to 23% yield from the ozonolysis of isoprene, is a four carbon, asymmetric, resonance-stabilized Criegee intermediate (Barber et al., 2018). MVK-OO has four conformers, *syn-trans*-, *syn-cis*-, *anti-trans*-, and *anti-cis*- as shown in Fig. S10. Herein, *syn* and *anti* refer to the orientation of the –CH$_3$ group relative to the terminal oxygen of MVK-OO, whereas *cis* and *trans* refer to the orientation of the C$_8$=C$_9$ bond relative to the C$_1$=O$_2$ bond. According to the results shown in the Fig. S10, the lowest-energy conformer is *syn-trans*-MVK-OO, which is lower than *syn-cis*-, *anti-trans*-, and *anti-cis*-MVK-OO by 1.42, 2.43 and 2.69 kcal·mol^{-1}, respectively. Therefore, the lowest-energy conformer *syn-trans*-MVK-OO is selected as the model compound to study its bimolecular reactions. As shown in Table 2, the rate coefficient of H$_2$O reaction with *syn-trans*-MVK-OO is lower than with other SCIs by 2 to 3 orders of magnitude. The reason is likely to be that the existence of methyl and vinyl

631 groups hinders the occurrence of bimolecular reaction with water vapour.

632 Consequently, a fraction of *syn-trans*-MVK-OO may survive in the presence of water

633 vapour and react with other species. $k_{eff(MVK-OO+H2O)}$ is nearly identical to

634 $k_{eff(MVK-OO+HCOOH)}$, which is greater than $k_{eff(MVK-OO+SO2)}$, which, in turn, is greater than

635 $k_{eff(MVK-OO+HPMF)}$ when the concentration of HPMF is equal to the atmospheric

636 concentration of SCIs. Based on the above discussions, it can be concluded that the

637 reactions of SCIs with HPMF is of minor importance in the atmosphere. These

638 reactions may play a certain role in the formation and growth of organic new particle

639 in some regions where low concentration of water vapour and high concentration of

640 hydroperoxide esters occur.
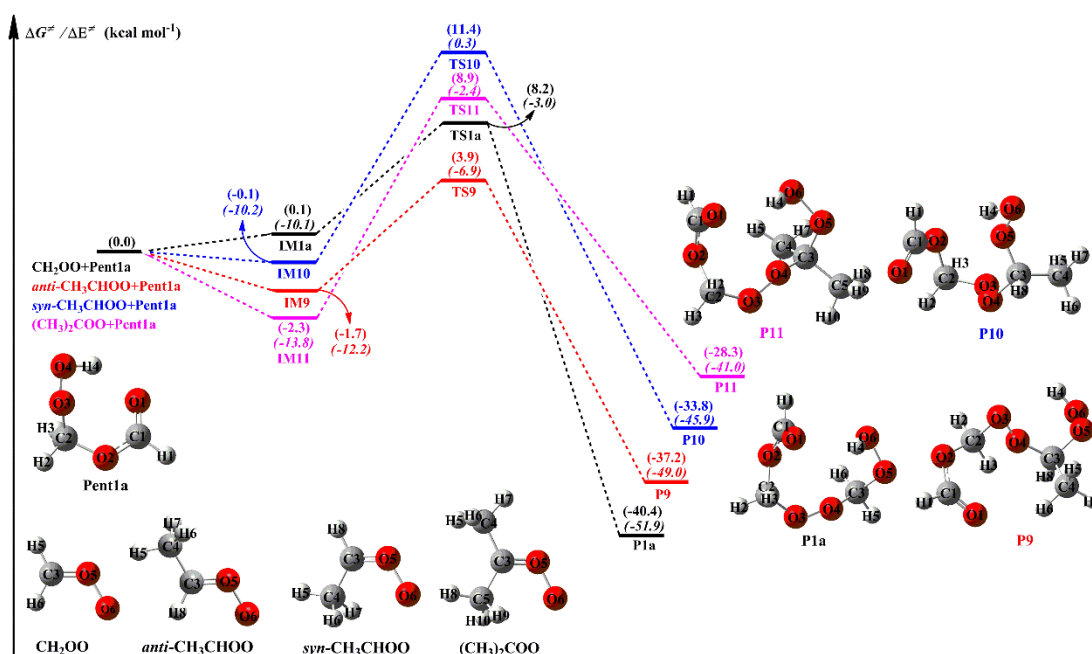
642 **Figure 6.** PES (ΔG and ΔE, in italics) for the distinct SCIs + Pent1a reactions at the
643 M06-2X/ma-TZVP//M06-2X/6-311+G(2df,2p) level of theory

645 **Table 2** The reported concentrations of coreactant, the rate coefficients k, and the effective
646 pseudo-first-order rate constants ($k_{eff} = k$[coreactant]) for distinct SCI reactions with HPMF, H$_2$O,
647 HCOOH and SO$_2$ at the tropical forest environments

SCIs	Coreactant	[Coreactant] (molecules cm^{-3})	k (cm^3 molecule^{-1} s^{-1})	k_{eff} (s^{-1})	Reference
CH$_2$OO	H$_2$O	3.9-6.1 × 10^{17}	< 1.5 × 10^{-15}	5.9-9.2 × 10^2	Chao et al., (2015)
	HCOOH	5.0-10.0 × 10^{10}	[1.1 ± 0.1] × 10^{-10}	5.5-11	Welz et al., (2014)

	SO$_2$	1.7-9.0 × 10^{10}	[3.9 ± 0.7] × 10^{-11}	0.7-3.5	Welz et al., (2012)
	HPMF	-	2.7 × 10^{-11}	-	This work
	H$_2$O	3.9-6.1 × 10^{17}	[1.0 ± 0.4] × 10^{-14}	3.9-6.1 × 10^3	Taatjes et al., (2013)
anti-CH$_3$CHOO	HCOOH	5.0-10.0 × 10^{10}	[5 ± 3] × 10^{-10}	25.0-50.0	Welz et al., (2014)
	SO$_2$	1.7-9.0 × 10^{10}	[6.7 ± 1.0] × 10^{-11}	1.1-6.0	Taatjes et al., (2013)
	HPMF	-	3.3 × 10^{-10}	-	This work
	H$_2$O	3.9-6.1 × 10^{17}	< 4.0 × 10^{-15}	1.6-2.4 × 10^3	Taatjes et al., (2013)
syn-CH$_3$CHOO	HCOOH	5.0-10.0 × 10^{10}	[2.5 ± 0.3] × 10^{-10}	12.5-25.0	Welz et al., (2014)
	SO$_2$	1.7-9.0 × 10^{10}	[2.4 ± 0.3] × 10^{-11}	0.4-2.2	Taatjes et al., (2013)
	HPMF	-	1.7 × 10^{-13}	-	This work
	H$_2$O	3.9-6.1 × 10^{17}	< 1.5 × 10^{-16}	58.5-91.5	Huang et al., (2015)
(CH$_3$)$_2$COO	HCOOH	5.0-10.0 × 10^{10}	4.5 × 10^{-10}	22.5-45.0	Sipilä et al., (2014)
	SO$_2$	1.7-9.0 × 10^{10}	1.3 × 10^{-10}	2.2-11.7	Huang et al., (2015)
	HPMF	-	2.2 × 10^{-11}	-	This work
	H$_2$O	3.9-6.1 × 10^{17}	< 4.0 × 10^{-17}	15.6-24.4	Caravan et al., (2020)
syn-trans-MVK-OO	HCOOH	5.0-10.0 × 10^{10}	[3.0 ± 0.1] × 10^{-10}	15.0-30.0	Caravan et al., (2020)
	SO$_2$	1.7-9.0 × 10^{10}	[4.2 ± 0.6] × 10^{-11}	0.7-3.8	Caravan et al., (2020)
	HPMF	-	3.0 × 10^{-11}	-	This work

3.4 Vapour pressure and volatility of the adduct products

The saturated vapour pressure (P^0) of the adduct products formed from the successive reactions of SCIs with HCOOH is estimated by using the EVAPORATION method proposed by Compernolle et al. (2011), and the room temperature results are

652 summarized in Table S8. This table shows that the P^0 of the adduct products decreases

653 significantly as the number of SCIs is increased. Notably, the P^0 of the adduct

654 products decreases when the size of SCIs increases. For example, the P^0 of the adduct

655 product $HC(O)O(CH_2OO)_3H$ in the nCH_2OO + HCOOH reaction is estimated to be

656 3.41×10^{-5} atm, which is greater than those of the corresponding adduct products in

657 the n$anti$-CH_3CHOO + HCOOH (4.73×10^{-6} atm), nsyn-CH_3CHOO + HCOOH (4.73

658 $\times 10^{-6}$ atm), and $n(CH_3)_2COO$ + HCOOH (1.03×10^{-6} atm) reactions by 7.21, 7.21

659 and 33.11 times, respectively.

660   A classify scheme of various organic compounds is based on their volatility, as

661 presented by Donahue et al. (2012) The volatility of organic compounds is described

662 by their effective saturation concentrations. The saturated concentrations (c^0) of the

663 adduct products formed from the successive reactions of SCIs with HCOOH are listed

664 in Table S8. As shown in Table S8, the c^0 of the adduct products decrease significantly

665 as the number of SCIs is increased. It deserves mentioning that the c^0 of the adduct

666 products decrease with increasing the size of SCIs. For the nCH_2OO + HCOOH

667 reaction, the c^0 of the adduct products are estimated to be 1.03×10^8 (n=1), 5.42×10^6

668 (n=2), 2.53×10^5 (n=3), 1.11×10^4 (n=4) and 4.67×10^2 (n=5) ug/m^3, respectively.

669 According to the Volatility Basis Set (VBS) of organic compounds (Donahue et al.,

670 2012), the adduct products belong to volatile organic compounds (VOC, $c^0 > 3 \times 10^6$

671 ug/m^3) when the number of SCIs is less than or equal to two, while they belong to

672 intermediate volatility organic compounds (IVOC, $300 < c^0 < 3 \times 10^6$ ug/m^3) when

673 the number of SCIs is greater than or equal to three. Similarly, the adduct products in

674 the n$anti$-CH_3CHOO + HCOOH, nsyn-CH_3CHOO + HCOOH, and $n(CH_3)_2COO$ +

675 HCOOH reactions belong to IVOC when the number of SCIs ranges from 2 to 4,

676 whereas they belong to semivolatile organic compounds (SVOC, $0.3 < c^0 < 300$ ug/m^3)

677 when the number of SCIs is equal to 5. Based on the above discussions, it can be

678 concluded that the volatility of the adduct products is significantly affected by the

679 number and size of SCIs in the successive reaction of SCIs with HCOOH. The formed

680 adduct products may participate in the formation and growth processes of organic new

681 particle in the atmosphere.

4. Conclusions

The oligomerization reaction mechanism and kinetics of Criegee intermediates reactions with their respective hydroperoxide esters as well as HPMF are investigated using quantum chemical calculations and kinetics modeling methods. The main conclusion is summarized as follows.

(a) For the initiation reactions of distinct SCIs with HCOOH, the barrierless 1,4 O-H insertion reaction leading to the formation of hydroperoxide esters is the most favorable pathway. The exothermicity of distinct SCIs reactions with HCOOH decreases when the number of methyl groups increases, and the exothermicity of the *anti*-CH$_3$CHOO + HCOOH reaction is higher than that of the *syn*-CH$_3$CHOO + HCOOH system.

(b) The addition reactions of SCIs with hydroperoxide esters proceed through successive insertion of SCIs into hydroperoxide ester to form oligomers that involve SCIs as the repeating unit. These oligomerization reactions are strongly exthermoic and spontaneous. The exothermicity of oligomerization reactions significantly decreases when the number of methyl substituents increases, and the exothermicity of *anti*-methyl substituted carbonyl oxides is higher than that of *syn*-methyl substituted carbonyl oxides.

(c) The –OOH insertion reaction is favored over the –CH insertion pathway in the SCIs oligomerization reactions, and the barrier heights increase with increasing the number of SCIs added to the oligomer except *syn*-CH$_3$CHOO. The barrier of -OOH insertion pathway shows a dramatic decrease when a methyl substituent occurs at the *anti*-position, while it reveals a significant increase when a methyl group is introduced at the *syn*-position and dimethyl substituent.

(d) Compared with the barrier of CH$_2$OO reaction with HPMF (8.1 kcal·mol^{-1}), the barrier decreases by 2.5 kcal·mol^{-1} when a methyl substituent occurs at the *anti*-position, while the barrier increases by about 3.0 kcal·mol^{-1} when a methyl group is introduced at the *syn*-position and dimethyl substituent. The rate coefficients increase by about one order of magnitude when a methyl substituent occurs at the

anti-position, whereas the rate coefficients decrease by 1 to 2 orders of magnitude when a methyl group is introduced at the *syn*-position compared to the rate coefficients of the CH_2OO + HPMF reaction.

(e) In the tropical forest environments, the effective pseudo-first-order rate constants for the reactions of distinct SCIs with HPMF ($k_{eff(SCIs+HPMF)}$) are several orders of magnitude lower than those for the reactions of distinct SCIs with H_2O ($k_{eff(SCIs+H2O)}$), HCOOH ($k_{eff(SCIs+HCOOH)}$) and SO_2 ($k_{eff(SCIs+SO2)}$). $k_{eff(SCIs+H2O)}$ is greater than $k_{eff(SCIs+HCOOH)}$, which, in turn, is greater than $k_{eff(SCIs+SO2)}$.

(f) The saturated vapour pressure and saturated concentration of the adduct products formed from the successive reactions of SCIs with HCOOH decrease significantly as the number of SCIs is increased. The adduct products in the nCH_2OO + HCOOH reactions belong to IVOC when the number of SCIs is greater than or equal to 3. The adduct products in the n*anti*-CH_3CHOO + HCOOH, n*syn*-CH_3CHOO + HCOOH, and $n(CH_3)_2COO$ + HCOOH reactions belong to IVOC when the number of SCIs ranges from 2 to 4, whereas they belong to SVOC when the number of SCIs is equal to 5.

Data availability

The data are accessible by contacting the corresponding author (huangyu@ieecas.cn).

Supplement

The following information is provided in the Supplement: The electronic energy ($\Delta E^{\neq}$) and Gibbs free energy ($\Delta G^{\neq}$) barriers for the initiation reactions of distinct SCIs with HCOOH predicted at different levels; Enthalpies of formation for the various carbonyl oxides and hydroperoxide esters; Rate coefficients of initiation reactions of distinct SCIs with HCOOH; Rate coefficients of distinct SCIs reactions with HPMF; Predicted saturated vapour pressure (P^0) and saturated concentrations (c^0) for the adduct products; Electronic potential energy along the O-H and C-O distance

calculated by the M06-2X/6-311+G(2df,2p) method for the barrierless 1,4-insertion reactions; Natural bond orbital (NBO) analysis of the donor-acceptor orbitals involved in the TS1a; The NPA charges of different atoms in the distinct SCIs; Optimized geometries of all the stationary points.

Author contribution

LC designed the study. LC and YH wrote the paper. LC performed theoretical calculation. YX, ZJ, and WW analyzed the data. All authors reviewed and commented on the paper.

Competing interests

The authors declare that they have no conflict of interest.

Acknowledgments

We thank Dr. Makroni Lily for valuable discussions on the barrierless 1,4 O-H insertion reactions. This work was supported by the National Natural Science Foundation of China (grant Nos. 42175134, 41805107, and 22002080). It was also partially supported as Strategic Priority Research Program of the Chinese Academy of Sciences, China (grant Nos. XDA23010300 and XDA23010000), and CAS "Light of West China" Program (XAB2019B01).

References

Alecu, I. M., Zheng, J., Zhao, Y., and Truhlar, D. G.: Computational thermochemistry: scale factor databases and scale factors for vibrational frequencies obtained from electronic model chemistries, J. Chem. Theory Comput., 6, 2872-2887, https://doi.org/10.1021/ct100326h, 2010.

Anglada, J. M., and Solé, A.: Impact of the water dimer on the atmospheric reactivity of carbonyl oxides, Phys. Chem. Chem. Phys., 18, 17698-17712, https://doi.org/10.1039/C6CP02531E, 2016.

Aplincourt, P., and Ruiz-López, M. F.: Theoretical study of formic acid anhydride formation from carbonyl oxide in the atmosphere, J. Phys. Chem. A, 104, 380-388, https://doi.org/10.1021/jp9928208, 2000.

Atkinson, R., and Arey, J.: Atmospheric degradation of volatile organic compounds, Chem. Rev., 103, 4605-4638, https://doi.org/10.1021/cr0206420, 2003.

Bao, J. L., and Truhlar, D. G.: Variational transition state theory: theoretical framework and recent developments, Chem. Soc. Rev., 46, 7548-7596, https://doi.org/10.1039/c7cs00602k, 2017.

Barber, V. P., Pandit, S., Green, A. M., Trongsiriwat, N., Walsh, P. J., Klippenstein, S. J., and Lester, M. I.: Four-carbon Criegee intermediate from isoprene ozonolysis: methyl vinyl ketone oxide synthesis, infrared spectrum, and OH production, J. Am. Chem. Soc., 140, 10866-10880, https://doi.org/10.1021/jacs.8b06010, 2018.

Boys, S. F., and Bernardi, F.: The calculation of small molecular interactions by the differences of separate total energies. Some procedures with reduced errors, Mol. Phys., 19, 553-566, https://doi.org/10.1080/00268977000101561, 1970.

Cabezas, C., and Endo, Y.: Observation of hydroperoxyethyl formate from the reaction between the methyl Criegee intermediate and formic acid, Phys. Chem. Chem. Phys., 22, 446-454, https://doi.org/10.1039/C9CP05030B, 2020.

Cabezas, C., and Endo, Y.: The Criegee intermediate-formic acid reaction explored by rotational spectroscopy, Phys. Chem. Chem. Phys., 21, 18059-18064, https://doi.org/10.1039/c9cp03001h, 2019.

Cabezas, C., and Endo, Y.: The reactivity of the Criegee intermediate CH_3CHOO with water probed by FTMW spectroscopy, J. Chem. Phys., 148, 014308-014315, https://doi.org/10.1063/1.5009033, 2018.

Canneaux, S., Bohr, F., and Henon, E.: KiSThelP: a program to predict thermodynamic properties and rate constants from quantum chemistry results, J. Comput. Chem., 35, 82-93, https://doi.org/10.1002/jcc.23470, 2013.

Caravan, R. L., Vansco, M. F., Au, K., Khan, M. A. H., Li, Y. L., Winiberg, F. A. F., Zuraski, K., Lin, Y. H., Chao, W., Trongsiriwat, N., Walsh, P. J., Osborn, D. L., Percival, C. J., Lin, J. J. M., Shallcross, D. E., Sheps, L., Klippenstein, S. J., Taatjes, C. A., and Lester, M. I.: Direct kinetic measurements and theoretical predictions of an isoprene-derived Criegee intermediate, Proc. Natl. Acad. Sci. U.S.A., 117, 9733-9740, https://doi.org/10.1073/pnas.1916711117, 2020.

Chaliyakunnel, S., Millet, D. B., Wells, K. C., Cady-Pereira, K. E., and Shephard, M. W.: A large underestimate of formic acid from tropical fires: constraints from space-borne measurements, Environ. Sci. Technol., 50, 5631-5640, https://doi.org/10.1021/acs.est.5b06385, 2016.

Chao, W., Hsieh, J. T., Chang, C. H., and Lin, J. J. M.: Direct kinetic measurement of the reaction of the simplest Criegee intermediate with water vapor, Science, 347, 751-754, https://doi.org/10.1126/science.1261549, 2015.

Chen, L., Huang, Y., Xue, Y., Cao J., and Wang, W.: Effect of oligomerization reactions of Criegee intermediate with organic acid/peroxy radical on secondary organic aerosol formation from isoprene ozonolysis, Atmos. Environ., 187, 218-229, https://doi.org/10.1016/j.atmosenv.2018.06.001, 2018.

Chen, L., Huang, Y., Xue, Y., Cao, J., and Wang, W.: Competition between HO_2 and H_2O_2 reactions with CH_2OO/*anti*-CH_3CHOO in the oligomer formation: a theoretical perspective, J. Phys. Chem. A, 121, 6981-6991, https://doi.org/10.1021/acs.jpca.7b05951, 2017.

Chen, L., Huang, Y., Xue, Y., Shen, Z., Cao, J., and Wang, W.: Mechanistic and kinetics investigations of oligomer formation from Criegee intermediate reactions with hydroxyalkyl hydroperoxides, Atmos. Chem. Phys., 19, 4075-4091, https://doi.org/10.5194/acp-19-4075-2019, 2019.

Chen, L., Wang, W., Wang, W., Liu, Y., Liu, F., Liu, N., and Wang, B: Water-catalyzed decomposition of the simplest Criegee intermediate CH_2OO, Theor. Chem. Acc., 135, 131-143, https://doi.org/10.1007/s00214-016-1894-9, 2016.

Chhantyal-Pun, R., McGillen, M. R., Beames, J. M., Khan, M. A. H., Percival, C. J., Shallcross, D. E., and Orr-Ewing, A. J.: Temperature Dependence of the Rates of Reaction of Trifluoracetic Acid with Criegee Intermediates, Angew. Chem. Int. Ed., 129, 9172-9175, https://doi.org/10.1002/anie.201703700, 2017.

Chhantyal-Pun, R., Rotavera, B., Mcgillen, M. R., Khan, M. A. H., Eskola, A. J., Caravan, R. L., Blacker, L., Tew, D. P., Osborn, D. L., Percival, C. J., Taatjes, C. A., Shallcross D. E., and Orr-Ewing, A. J.: Criegee intermediate reactions with carboxylic acids: a potential source of secondary organic aerosol in the atmosphere, ACS Earth Space Chem., 2, 833-842, https://doi.org/10.1021/acsearthspacechem.8b00069, 2018.

Chung, C. A., Su, J. W., and Lee, Y. P.: Detailed mechanism and kinetics of the reaction of Criegee intermediate CH_2OO with HCOOH investigated via infrared identification of conformers of hydroperoxymethyl formate and formic acid anhydride, Phys. Chem. Chem. Phys., 21, 21445-21455, https://doi.org/10.1039/c9cp04168k, 2019.

Compernolle, S., Ceulemans, K., and Müller, J. F.: EVAPORATION: a new vapour pressure estimation method for organic molecules including non-additivity and intramolecular interactions, Atmos. Chem. Phys., 11, 9431-9450, https://doi.org/10.5194/acp-11-9431-2011, 2011.

Criegee, R.: Mechanism of ozonolysis, Angew. Chem. Int. Ed. Engl., 14, 745-752, https://doi.org/10.1002/anie.197507451, 1975.

Donahue, N. M., Kroll, J. H., Pandis, S. N., and Robinson, A. L.: A two-dimensional volatility basis set – Part 2: Diagnostics of organic-aerosol evolution, Atmos. Chem. Phys., 12, 615-634, https://doi.org/10.5194/acp-12-615-2012, 2012.

Drozd, G. T., Kurtén, T., Donahue, N. M., and Lester, M. I.: Unimolecular decay of the dimethyl-substituted Criegee intermediate in alkene ozonolysis: decay time scales and the importance of tunneling, J. Phys. Chem. A, 121, 6036-6045, https://doi.org/10.1021/acs.jpca.7b05495, 2017.

Eckart, C.: The penetration of a potential barrier by electrons, Phys. Rev., 35, 1303-1309,

849   https://doi.org/10.1103/PhysRev.35.1303, 1930.

850 Frisch, M. J., Trucks, G. W., Schlegel, H. B., Scuseria, G. E., Robb, M. A., Cheeseman, J. R.,
851   Montgomery, J. A. Jr., Vreven, T., Kudin, K. N., Burant, J. C., Millam, J. M., Iyengar, S. S.,
852   Tomasi, J., Barone, V., Mennucci. B., Cossi, M., Scalmani, G., Rega, N., Petersson, G. A.,
853   Nakatsuji, H., Hada, M., Ehara, M., Toyota, K., Fukuda, R., Hasegawa, J., Ishida, M.,
854   Nakajima, T., Honda, Y., Kitao, O., Nakai, H., Klene, M., Li, X., Knox, J. E., Hratchian, H. P.,
855   Cross, J. B., Adamo, C., Jaramillo, J., Gomperts, R., Stratmann, R. E., Yazyev, O., Austin, A.
856   J., Cammi, R., Pomelli, C., Ochterski, J. W., Ayala, P. Y., Morokuma, K., Voth, G. A.,
857   Salvador, P., Dannenberg, J. J., Zakrzewski, V. G., Dapprich, S., Daniels, A. D., Strain, M. C.,
858   Farkas, O., Malick, D. K., Rabuck, A. D., Raghavachari, K., Foresman, J. B., Ortiz, J. V., Cui,
859   Q., Baboul, A. G., Clifford, S., Cioslowski, J., Stefanov, B. B., Liu, G., Liashenko, A.,
860   Piskorz, P., Komaromi, I., Martin, R. L., Fox, D. J., Keith, T., Al-Laham, M. A., Peng, C. Y.,
861   Nanayakkara, A., Challacombe, M., Gill, P. M. W., Johnson, B., Chen, W., Wong, M. W.,
862   Gonzalez, C., and Pople, J. A.: Gaussian 09, Revision D.01; Gaussian, Inc.: Wallingford, CT,
863   2009.

864 Fukui, K.: The path of chemical reactions - the IRC approach, Acc. Chem. Res., 14, 363-368,
865   https://doi.org/10.1021/ar00072a001, 1981.

866 Giorio, C., Campbell, S. J., Bruschi, M., Tampieri, F., Barbon, A., Toffoletti, A., Tapparo, A.,
867   Paijens, C., Wedlake, A. J., Grice, P., Howe, D. J., and Kalbere, M.: Online quantification of
868   Criegee intermediates of α-pinene ozonolysis by stabilization with spin traps and
869   proton-transfer reaction mass spectrometry detection, J. Am. Chem. Soc., 139, 3999-4008,
870   https://doi.org/10.1021/jacs.6b10981, 2017.

871 Gong, Y., and Chen, Z.: Quantification of the role of stabilized Criegee intermediates in the
872   formation of aerosols in limonene ozonolysis, Atmos. Chem. Phys., 21, 813-829,
873   https://doi.org/10.5194/acp-21-813-2021, 2021.

874 Hammond, G. S.: A correlation of reaction rates, J. Am. Chem. Soc., 77, 334-338,
875   https://doi.org/10.1021/ja01607a027, 1955.

876 Huang, H. L., Chao, W., and Lin, J. J. M.: Kinetics of a Criegee intermediate that would survive
877   high humidity and may oxidize atmospheric SO_2, Proc. Natl. Acad. Sci. U.S.A., 112,
878   10857-10862, https://doi.org/ 10.1073/pnas.1513149112, 2015.

879 Humphrey, W., Dalke, A., and Schulten, K.: VMD: Visual molecular dynamics, J. Molec.
880   Graphics, 14, 33-38, https://doi.org/10.1016/0263-7855(96)00018-5, 1996.

881 Johnson, D., and Marston, G.: The gas-phase ozonolysis of unsaturated volatile organic
882   compounds in the troposphere, Chem. Soc. Rev., 37, 699-716,
883   https://doi.org/10.1039/B704260B, 2008.

884 Johnson, D., Lewin, A. G., and Marston, G.: The effect of Criegee-intermediate scavengers on the
885   OH yield from the reaction of ozone with 2-methylbut-2-ene, J. Phys. Chem. A, 105,
886   2933-2935, https://doi.org/10.1021/jp003975e, 2001.

887 Karton, A., Kettner, M., and Wild, D. A.: Sneaking up on the Criegee intermediate from below:
888   Predicted photoelectron spectrum of the CH_2OO^- anion and W3-F12 electron affinity of
889   CH_2OO, Chem. Phys. Lett., 585, 15-20, https://doi.org/10.1016/j.cplett.2013.08.075, 2013.

890 Khan, M. A. H., Percival, C. J., Caravan, R. L., Taatjes, C. A., and Shallcross, D. E.: Criegee
891   intermediates and their impacts on the troposphere, Environ. Sci.: Processes Impacts, 20,
892   437-453, https://doi.org/10.1039/C7EM00585G, 2018.

Lester, M. I., and Klippenstein, S. J.: Unimolecular decay of Criegee intermediates to OH radical products: prompt and thermal decay processes, Acc. Chem. Res., 51, 978-985, https://doi.org/10.1021/acs.accounts.8b00077, 2018.

Lin, J. J. M., and Chao, W.: Structure-dependent reactivity of Criegee intermediates studied with spectroscopic methods, Chem. Soc. Rev., 46, 7483-7497, https://doi.org/10.1039/c7cs00336f, 2017.

Lin, X., Meng, Q., Feng, B., Zhai, Y., Li, Y., Yu, Y., Li, Z., Shan, X., Liu, F., Zhang, L., and Sheng, L.: Theoretical study on Criegee intermediate's role in ozonolysis of acrylic acid, J. Phys. Chem. A, 123, 1929-1936, https://doi.org/10.1021/acs.jpca.8b11671, 2019.

Liu, F., Beames, J. M., Petit, A. S., McCoy, A. B., and Lester, M. I.: Infrared-driven unimolecular reaction of CH_3CHOO Criegee intermediates to OH radical products, Science, 345, 1596-1598, https://doi.org/10.1126/science.1257158, 2014.

Liu, L., Bei, N., Wu, J., Liu, S., Zhou, J., Li, X., Yang, Q., Feng, T., Cao, J., Tie, X., and Li, G.: Effects of stabilized Criegee intermediates (sCIs) on sulfate formation: a sensitivity analysis during summertime in Beijing-Tianjin-Hebei (BTH), China, Atmos. Chem. Phys., 19, 13341-13354, https://doi.org/10.5194/acp-19-13341-2019, 2019.

Long, B., Bao, J. L., and Truhlar, D. G.: Atmospheric chemistry of Criegee intermediates: unimolecular reactions and reactions with water, J. Am. Chem. Soc., 138, 14409-14422, https://doi.org/10.1021/jacs.6b08655, 2016.

Long, B., Bao, J. L., and Truhlar, D. G.: Unimolecular reaction of acetone oxide and its reaction with water in the atmosphere, Proc. Natl. Acad. Sci. U.S.A., 115, 6135-6140, https://doi.org/10.1073/pnas.1804453115, 2018.

Long, B., Cheng, J. R., Tan, X. F., and Zhang, W. J.: Theoretical study on the detailed reaction mechanisms of carbonyl oxide with formic acid, J. Mol. Struc.: Theochem, 916, 159-167, https://doi.org/10.1016/j.theochem.2009.09.028, 2009.

Lu, T., and Chen, F.: Multiwfn: A multifunctional wavefunction analyzer, J. Comput. Chem., 33, 580-592, https://doi.org/10.1002/jcc.22885, 2012.

Mendes, J., Zhou, C. W., and Curran, H. J.: Theoretical chemical kinetic study of the H-atom abstraction reactions from aldehydes and acids by H atoms and OH, HO_2, and CH_3 radicals, J. Phys. Chem. A, 118, 12089-12104, https://doi.org/10.1021/jp5072814, 2014.

Neeb, P., Horie, O., and Moortgat, G. K.: The ethene-ozone reaction in the gas phase, J. Phys. Chem. A, 102, 6778-6785, https://doi.org/10.1021/jp981264z, 1998.

Novelli, A., Hens, K., Ernest, C. T., Martinez, M., Nölscher, A. C., Sinha, V., Paasonen, P., Petäjä, T., Sipilä, M., Elste, T., Plass-Dülmer, C., Phillips, G. J., Kubistin, D., Williams, J., Vereecken, L., Lelieveld, J., and Harder, H.: Estimating the atmospheric concentration of Criegee intermediates and their possible interference in a FAGE-LIF instrument, Atmos. Chem. Phys., 17, 7807-7826, https://doi.org/10.5194/acp-17-7807-2017, 2017.

Novelli, A., Vereecken, L., Lelieveld, J., and Harder, H.: Direct observation of OH formation from stabilised Criegee intermediates, Phys. Chem. Chem. Phys., 16, 19941-19951, https://doi.org/10.1039/c4cp02719a, 2014.

Osborn, D. L., and Taatjes, C. A.: The physical chemistry of Criegee intermediates in the gas phase, Int. Rev. Phys. Chem., 34, 309-360, https://doi.org/10.1080/0144235X.2015.1055676, 2015.

Paulot, F., Wunch, D., Crounse, J. D., Toon, G. C., Millet, D. B., DeCarlo, P. F., Vigouroux, C.,

937 Deutscher, N. M., Abad, G. G., Notholt, J., Warneke, T., Hannigan, J. W., Warneke, C., de
938 Gouw, J. A., Dunlea, E. J., Mazière, M. D., Griffith, D. W. T., Bernath, P., Jimenez, J. L., and
939 Wennberg, P. O.: Importance of secondary sources in the atmospheric budgets of formic and
940 acetic acids, Atmos. Chem. Phys., 11, 1989-2013, https://doi.org/10.5194/acp-11-1989-2011,
941 2011.

942 Peltola, J., Seal, P., Inkilä, A., and Eskola, A.: Time-resolved, broadband UV-absorption
943 spectrometry measurements of Criegee intermediate kinetics using a new photolytic
944 precursor: unimolecular decomposition of CH_2OO and its reaction with formic acid, Phys.
945 Chem. Chem. Phys., 22, 11797-11808, https://doi.org/10.1039/d0cp00302f, 2020.

946 Porterfield, J. P., Lee, K. L. K., Dell'Isola, V., Carroll, P. B., and McCarthy, M. C.:
947 Characterization of the simplest hydroperoxide ester, hydroperoxymethyl formate, a
948 precursor of atmospheric aerosols, Phys. Chem. Chem. Phys., 21, 18065-18070,
949 https://doi.org/10.1039/c9cp03466h, 2019.

950 Riva, M., Budisulistiorini, S. H., Zhang, Z., Gold, A., Thornton, J. A., Turpin, B. J., and Surratt, J.
951 D.: Multiphase reactivity of gaseous hydroperoxide oligomers produced from isoprene
952 ozonolysis in the presence of acidified aerosols, Atmos. Environ., 152, 314-322,
953 https://doi.org/10.1016/j.atmosenv.2016.12.040, 2017.

954 Sadezky, A., Winterhalter, R., Kanawati, B., Rompp, A., Spengler, B., Mellouki, A., Bras, G. L.,
955 Chaimbault, P., and Moortgat, G. K.: Oligomer formation during gas-phase ozonolysis of
956 small alkenes and enol ethers: new evidence for the central role of the Criegee Intermediate
957 as oligomer chain unit, Atmos. Chem. Phys., 8, 2667-2699,
958 https://doi.org/10.5194/acp-8-2667-2008, 2008.

959 Sakamoto, Y., Inomata, S., and Hirokawa, J.: Oligomerization reaction of the Criegee intermediate
960 leads to secondary organic aerosol formation in ethylene ozonolysis, J. Phys. Chem. A, 117,
961 12912-12921, https://doi.org/10.1021/jp408672m, 2013.

962 Sakamoto, Y., Yajima, R., Inomatad, S., and Hirokawa, J.: Water vapour effects on secondary
963 organic aerosol formation in isoprene ozonolysis, Phys. Chem. Chem. Phys., 19, 3165-3175,
964 https://doi.org/10.1039/c6cp04521a, 2017.

965 Sipilä, M., Jokinen, T., Berndt, T., Richters, S., Makkonen, R., Donahue, N. M., Mauldin Iii, R. L.,
966 Kurtén, T., Paasonen, P., Sarnela, N., Ehn, M., Junninen, H., Rissanen, M. P., Thornton, J.,
967 Stratmann, F., Herrmann, H., Worsnop, D. R., Kulmala, M., Kerminen, V. M., and Petäjä, T.:
968 Reactivity of stabilized Criegee intermediates (sCIs) from isoprene and monoterpene
969 ozonolysis toward SO_2 and organic acids, Atmos. Chem. Phys., 14, 12143-12153,
970 https://doi.org/10.5194/acp-14-12143-2014, 2014.

971 So, S., Wille, U., and Silva, G. D.: Atmospheric chemistry of enols: a theoretical study of the vinyl
972 alcohol + OH + O_2 reaction mechanism, Environ. Sci. Technol., 48, 6694-6701,
973 https://doi.org/10.1021/es500319q, 2014.

974 Stavrakou, T., Müller, J. F., Peeters, J., Razavi, A., Clarisse, L., Clerbaux, C., Coheur, P. F.,
975 Hurtmans, D., Mazière, M. D., Vigouroux, C., Deutscher, N. M., Griffith, D. W. T., Jones, N.,
976 and Paton-Walsh, C.: Satellite evidence for a large source of formic acid from boreal and
977 tropical forests, Nat. Geosci., 5, 26-30, https://doi.org/10.1038/ngeo1354, 2012.

978 Taatjes, C. A., Khan, M. A. H., Eskola, A. J., Percival, C. J., Osborn, D. L., Wallington, T. J., and
979 Shallcross, D. E.: Reaction of perfluorooctanoic acid with Criegee intermediates and
980 implications for the atmospheric fate of perfluorocarboxylic acids, Environ. Sci. Technol., 53,

981 1245-1251, https://doi.org/10.1021/acs.est.8b05073, 2019.

982 Taatjes, C. A., Welz, O., Eskola, A. J., Savee, J. D., Scheer, A. M., Shallcross, D. E., Rotavera, B.,
983 Lee, E. P. F., Dyke, J. M., Mok, D. K. W., Osborn, D. L., and Percival, C. J.: Direct
984 measurements of conformer-dependent reactivity of the Criegee intermediate CH_3CHOO,
985 Science, 340, 177-180, https://doi.org/10.1126/science.1234689, 2013.

986 Taatjes, C. A.: Criegee intermediates: what direct production and detection can teach us about
987 reactions of carbonyl oxides, Annu. Rev. Phys. Chem., 68, 183-207,
988 https://doi.org/10.1146/annurev-physchem-052516-050739, 2017.

989 Tobias, H. J., and Ziemann, P. J.: Kinetics of the gas-phase reactions of alcohols, aldehydes,
990 carboxylic acids, and water with the C13 stabilized Criegee intermediate formed from
991 ozonolysis of 1-tetradecene, J. Phys. Chem. A, 105, 6129-6135,
992 https://doi.org/10.1021/jp004631r, 2001.

993 Truhlar, D. G., Hase, W. L., and Hynes, J. T.: Current status of transition-state theory, J. Phys.
994 Chem., 87, 2664-2682, https://doi.org/10.1021/jp953748q, 1996.

995 Vansco, M. F., Zuraski, K., Winiberg, F. A. F., Au, K., Trongsiriwat, N., Walsh, P. J., Osborn, D. L.,
996 Percival, C. J., Klippenstein, S. J., Taatjes, C. A., Lester, M. I., and Caravan, R. L.:
997 Functionalized hydroperoxide formation from the reaction of methacrolein-oxide, an
998 isoprene-derived Criegee intermediate, with formic acid: experiment and theory, Molecules,
999 26, 3058-3072, https://doi.org/10.3390/molecules26103058, 2021.

1000 Vereecken, L., Harder, H., and Novelli, A.: The reaction of Criegee intermediates with NO, RO_2,
1001 and SO_2, and their fate in the atmosphere, Phys. Chem. Chem. Phys., 14, 14682-14695,
1002 https://doi.org/10.1039/c2cp42300f, 2012.

1003 Vereecken, L.: The reaction of Criegee intermediates with acids and enols, Phys. Chem. Chem.
1004 Phys., 19, 28630-28640, https://doi.org/10.1039/c7cp05132h, 2017.

1005 Wang, S., Newland, M. J., Deng, W., Rickard, A. R., Hamilton, J. F., Muñoz, A., Ródenas, M.,
1006 Vázquez, M. M., Wang, L., and Wang, X.: Aromatic photo-oxidation, a new source of
1007 atmospheric acidity, Environ. Sci. Technol., 54, 7798-7806,
1008 https://doi.org/10.1021/acs.est.0c00526, 2020.

1009 Welz, O., Eskola, A. J., Sheps, L., Rotavera, B., Savee, J. D., Scheer, A. M., Osborn, D. L., Lowe,
1010 D., Booth, A. M., Xiao, P., Khan, M. A. H., Percival, C. J., Shallcross, D. E., and Taatjes, C.
1011 A.: Rate coefficients of C(1) and C(2) Criegee intermediate reactions with formic and acetic
1012 Acid near the collision limit: direct kinetics measurements and atmospheric implications,
1013 Angew. Chem. Int. Ed., 53, 4547-4550, https://doi.org/10.1002/anie.201400964, 2014.

1014 Welz, O., Savee, J. D., Osborn, D. L., Vasu, S. S., Percival, C. J., Shallcross, D. E., and Taatjes, C.
1015 A.: Direct kinetic measurements of Criegee intermediate (CH_2OO) formed by reaction of
1016 CH_2I with O_2, Science, 335, 204-207, https://doi.org/10.1126/science.1213229, 2012.

1017 Yin, C., and Takahashi, K.: How does substitution affect the unimolecular reaction rates of
1018 Criegee intermediates? Phys. Chem. Chem. Phys., 19, 12075-12084,
1019 https://doi.org/10.1039/c7cp01091e, 2017.

1020 Yu, S.: Role of organic acids (formic, acetic, pyruvic and oxalic) in the formation of cloud
1021 condensation nuclei (CCN): a review, Atmos. Res., 53, 185-217,
1022 https://doi.org/10.1016/S0169-8095(00)00037-5, 2000.

1023 Zhang, P., Wang, W., Zhang, T., Chen, L., Du, Y., Li, C., and Lv, J.: Theoretical study on the
1024 mechanism and kinetics for the self-reaction of $C_2H_5O_2$ radicals, J. Phys. Chem. A, 116,

1025   4610-4620, https://doi.org/10.1021/jp301308u, 2012.

1026   Zhao, R., Kenseth, C. M., Huang, Y., Dalleska, N. F., Kuang, X. M., Chen, J., Paulson, S. E., and

1027   Seinfeld, J. H.: Rapid aqueous-phase hydrolysis of ester hydroperoxides arising from Criegee

1028   intermediates   and   organic   acids,   J.   Phys.   Chem.   A,   122,   5190-5201,

1029   https://doi.org/10.1021/acs.jpca.8b02195, 2018.

1030   Zhao, Y., and Truhlar, D. G.: The M06 suite of density functionals for main group

1031   thermochemistry, thermochemical kinetics, noncovalent interactions, excited states, and

1032   transition elements: two new functionals and systematic testing of four M06-class functionals

1033   and   12   other   functionals,   Theor.   Chem.   Acc.,   120,   215-241,

1034   https://doi.org/10.1007/s00214-007-0310-x, 2008.

1035   Zhao, Y., Wingen, L. M., Perraud, V., Greaves, J., and Finlayson-Pitts, B. J.: Role of the reaction

1036   of stabilized Criegee intermediates with peroxy radicals in particle formation and growth in

1037   air, Phys. Chem. Chem. Phys., 17, 12500-12514, https://doi.org/10.1039/c5cp01171j, 2015.

1038   Zheng, J., Bao, L. J., Meana-Paneda, R., Zhang, S., Lynch, B. J., Corchado, J. C., Chuang, Y. Y.,

1039   Fast, P. L., Hu, W. P., Liu, Y. P., Lynch, G. C., Nguyen, K. A., Jackels, C. F.,

1040   Fernandez-Ramos, A., Ellingson, B. A., Melissas, V. S., Villa, J., Rossi, I., Coitino, L., Pu, J.,

1041   Albu, T. V., Steckler, R., Garrett, B. C., Issacson, A. D., and Truhlar, D. G.: Polyrate, version

1042   2017-C, University of Minnesota: Minneapolis, MN, 2018.

1043   Zhou, S., Joudan, S., Forbes, M. W., Zhou, Z., and Abbatt, J. P. D.: Reaction of condensed-phase

1044   Criegee intermediates with carboxylic acids and perfluoroalkyl carboxylic acids, Environ. Sci.

1045   Technol. Lett., 6, 243-250, https://doi.org/10.1021/acs.estlett.9b00165, 2019.